Specialized neuronal modules for economic and single-attribute choice in the orbitofrontal cortex

Chengze Xu[1], Kuntan Ni[1], Xinying Cai[1,2,3]

Affiliations:
[1]NYU Shanghai, 1555 Century Avenue, Shanghai, 200122, China;
[2]Shanghai Key Laboratory of Brain Functional Genomics (Ministry of Education), School of Psychology and Cognitive Science, East China Normal University, Shanghai, 200062, China;
[3]NYU-ECNU Institute of Brain and Cognitive Science at NYU Shanghai, 3663 Zhongshan Road North, Shanghai, 200062, China

Keywords: economic choice, orbitofrontal cortex, subjective value, trade-off

Correspondence to:
Xinying Cai, Ph.D.
NYU Shanghai,
Tel: +86 (21) 20595157,
Email: xinying.cai@nyu.edu

Competing interests: The authors have no competing interests.

Acknowledgments: We thank Yuanyuan Liu for help with animal training and Camillo Padoa-Schioppa and Weikang Shi for helpful comments on the manuscript. This research was supported by National Science and Technology Innovation 2030 Major Program (No. 2021ZD0203700/2021ZD0203702 to X.C.) and Shanghai Municipal Science and Technology Major Project (2018SHZDZX05 to X.C.).

Abstract

An important aspect of biological intelligence is the ability of quick task switching. Such ability may be realized through a neural system equipped with functionally specialized modules subserving each task. The orbitofrontal cortex (OFC) harbors a persistent circuit supporting economic decisions under different contexts. To examine the specialization of this circuit, we contrasted the coding of the same neurons in the OFC of rhesus monkeys under economic choice (EC) and single-attribute choice (SC). In EC, OFC neurons largely encoded offer value, chosen value and choice outcome in goods space. Strikingly, these neurons were tuned out in SC while a complementary set of neurons encoded SC-related variables in a spatial reference frame. Moreover, in EC, neurons encoding the same value-related variable are anatomically clustered and the noise correlation among these neurons dropped significantly when the animal switched from EC to SC, suggesting altered functional organization. Thus, dedicated modules in the OFC may support cognitive flexibility in choice.

Introduction

Cognitive flexibility, such as task switching, is an important aspect of biological intelligence (Benedek et al., 2014; Salthouse et al., 1998). However, the underlying neural mechanism is still not well understood. One possibility is that such neural system consists of multiple functionally specialized modules and a particular module is recruited for the system to fulfill a particular task demand(Yang et al., 2019a; Yang et al., 2019b). An advantage of having functionally specialized modules is that structural knowledge of a task can be abstracted and generalized to instances under new sensory and/or motor contingencies (Behrens et al., 2018). In this regard, although seemingly paradoxical, circuit level functional specialization facilitates task generalization.

A broad range of experimental and theoretical studies have demonstrated flexible coding in the OFC in different choice contexts(Cai and Padoa-Schioppa, 2019; Conen and Padoa-Schioppa, 2019; Kobayashi et al., 2010; Padoa-Schioppa, 2009; Padoa-Schioppa and Assad, 2008; Rustichini et al., 2017; Tremblay and Schultz, 1999; Xie and Padoa-Schioppa, 2016). Meanwhile, the putative choice circuit has rarely been interrogated under different choice tasks therefore it remains unknown whether OFC harbors functionally specialized modules for different choice tasks.

Furthermore, although functional specialization has been proposed as one of the most fundamental organization principles of the brain(Kanwisher, 2010), little is known about functional specialization of task representations at the neuronal level as most of the studies so far have focused on the analysis of specialization regarding brain regions(Connolly et al., 2003; Conway et al., 2007; Downing et al., 2001; Gavrilov et al., 2017; Kanwisher et al., 1997; Tsao et al., 2006; Zeki, 1978). Neuronal level functional specialization is particularly pertinent to the prefrontal cortex (PFC) due to versatility in cognition. We speculate that task specialization in the PFC may manifest at a resolution finer than that suggested by previous studies(O'Reilly, 2010; Riley et al., 2017). Thus, cross task single-neuron analysis is critical in studying functional specialization of the PFC vis-à-vis higher cognitive functions.

To probe functional specialization of the OFC neuronal ensembles in reward-based decisions, we carried out a study in which monkeys switch between two different choice tasks, an economic choice task (EC) and a single attribute choice task (SC). In EC, the animal chose between two juices of variable amounts and the animal's choice pattern reflected a subjective tradeoff between juice taste and quantity. In SC, the animal chose between the same juice in different quantity, which is the only differentiating attribute for the two offers, and the animal's choice was directed towards the larger quantity offer deterministically. These different choice patterns suggested different mental operations under two choice tasks. Is each task supported by a 'private' cluster of neurons or the two processes share the same population of neurons?

To look into this question, we recorded the activity of the same neurons across the two tasks. In EC, OFC neurons encoded largely the same set of parameters as previously reported, namely, offer value, chosen value and chosen juice. Strikingly, after switching to SC, most of the EC-related neurons were tuned out. Meanwhile, a complementary set of neurons encoded SC-related variables. Thus, in the OFC, there seems to exist a doubly dissociated mapping between the putative neuronal modules and different mental operations for EC and SC. We further investigated whether these functional modules are supported by anatomical organizations of task-related neurons. We discovered that, in EC, value encoding neurons tend to exhibit anatomical clustering. Intriguingly, when the animal switched from EC to SC, there was also a significant reduction in the noise

correlations among the clustered value coding neurons, suggesting altered functional interactions, while their anatomical distance remained unchanged.

By contrasting the neuronal representations under EC and SC, our study provided the first physiological evidence supporting functionally specialized modules in the OFC representing decisions entailing distinct mental operations.

Results

Behavior

From the behavioral perspective, EC is characterized as entailing a tradeoff among competing attributes and preference towards these attributes is reflected in the idiosyncratic tradeoff patterns across decision makers as well as for the same decision maker under different circumstances. In the present study, we examined how neuronal representations in the OFC reconfigure when the animal switches from EC (A:B blocks) to SC (B:B and A:A blocks) (**Fig. 1a**). A typical experimental session includes four blocks of trials in the sequence of B:B, $(A:B)_1$, $(A:B)_2$, A:A (see **Methods**). Different juice pairs were offered in different experimental sessions and the same two juices were used throughout a single experimental session. To perform a matching analysis as that for the A:B block, for B:B blocks, in which the same juice was used for each offer, one of the two offers was coded as lowercase "a". By the same token, for A:A blocks, one of the two offers was coded as lowercase "b" (**Fig. 1b**). In the subsequent analysis, where applicable, $(A:B)_1$, and $(A:B)_2$ blocks are referred to as the A:B task , and B:B and A:A blocks are collectively referred to as the X:X task.

In the A:B task, the choice relative values are significantly larger than one for both animals (see **Methods**, **Fig. 1b**, monkey S (44 sessions), $\rho = 3.36 \pm 0.96$ (mean±std), $p < 10^{-19}$, t test; monkey N (59 sessions), $\rho = 1.75 \pm 0.35$ (mean±std), $p < 10^{-23}$, t test), while in the X:X task, the choice relative values are not significantly different from one for either animal (**Fig. 1b**, monkey S (46 sessions), $\rho = 1.005 \pm 0.029$ (mean±std), $p = 0.23$, t test; monkey N (51 sessions), $\rho = 0.999 \pm 0.023$ (mean±std), $p = 0.66$, t test). Moreover, in the X:X task, the animals' choice was dictated by offer quantity in that they chose the offer with larger quantity with high accuracy (**Fig. 1b**, monkey S: B:B condition (23 sessions), 97.7%±1.7%, A:A condition (23 sessions), 98.6%±1.2%; monkey N: B:B condition (34 sessions), 99.97%±0.16%, A:A condition (17 sessions), 100%±0%).

Contrasting the choice patterns between the A:B and X:X task suggests that the animals were engaged in distinct mental operations since in the A:B task, the animal's choice was driven by the comparison of the subjective values integrating both juice taste and quantity while in the X:X task, the choice is based on the comparison of the quantity of the same juice. Next, we investigated how these two distinct mental operations are represented in the OFC.

Neuronal coding in EC and SC

Our encoding analysis was based on 2029 cells in the A:B task and 1964 cells in the X:X task (see Methods). We first examined the encoding of task-related variables in the A:B and X:X task, respectively. We discovered that in the A:B task, OFC neurons largely encoded the same set of variables as previously reported, strikingly, most of them were tuned out when the animal switched to the X:X task.

Here, we show five example neurons in the A:B task (**Fig. 2**). One cell (**Fig. 2a**) encoded the Offer value of juice A; Similarly, another cell (**Fig. 2b**) encoded the Offer value of juice B. A third cell (**Fig. 2c**) encoded Chosen value. A fourth cell (**Fig. 2d**) encoded Chosen juice. A fifth cell encoded the number of square symbols on the contralateral hemifield (Symbol $\#_{contra}$). Importantly, few of these neurons encoded task-related variables in the X:X task.

Conversely, neurons encoding task-related variables in the X:X task switched to become untuned in the A:B task. We illustrate three example neurons here (**Fig. 3**). One cell (**Fig. 3a**) encoded the quantity of the contralateral offer (Offer $Quantity_{contra}$); Another cell (**Fig. 3b**) encoded the quantity of the chosen offer (Chosen Quantity) while a third cell encoded the location of the chosen offer (Chosen Side). Strikingly, all of these neurons became untuned in the A:B task.

For population analyses, we proceeded as follows. For the A:B task, a "trial type" was defined by two offers, their spatial configuration, and a choice (e.g., [1A+:3B-, A]). In this notation, "+" indicates offer locating on the left hemifield while "-" indicates offer locating on the right hemifield. For the X:X task, because there is only one type of juice and the animals almost always choose the offer with larger quantity, “trial type” was defined by two offers and the location of the larger quantity offer (e.g., [1B+:3B-]). Our neuronal analysis is focused on the post-offer window, which is defined as 100 ~ 600 ms after offer presentation. For each neuron, we conducted a 1-way ANOVA ($p<0.01$) across trial types. Neurons that passed the criterion were identified as task-related and included in subsequent variable selection analysis (350 out of 2029 cells (17.2%) in the A:B task, 157 out of 1964 cells (8%) in the X:X task).

Each neuronal response that passed the analysis of variance criterion was regressed against a set of variables that could potentially be encoded (**Table S1**). A variable was said to “explain” the response if the regression slope differed significantly from zero ($p < 0.05$). Each linear regression also provided the R^2. For variables that did not explain the response, we set $R^2=0$. The variable with the largest R^2 provided the “best fit” for the neuronal response and the cell was *untuned* if it did not encode any variable (see **Methods**). In the A:B task, overall, 308 of 350 (88%) task-related responses were explained by at least 1 of the 11 variables examined in the analysis (**Table S1**). For a quantitative assessment of the variables that best explained the population, we used the stepwise selection method. As illustrated in **Fig. 4a**, the first four iterations of this procedure selected variables Offer $Value_{juice}$, Chosen Value, Symbol $\#_{spatial}$ and Chosen Juice. Collectively, these four variables explained 92% (284/308) of the responses explained by the 11 variables. All variables selected in subsequent iterations provided a marginal explanatory power of < 5%. The best subset method confirmed that these four variables selected by the stepwise selection method explained more responses than any other subset of four variables. Neurons encoding each of these selected variables (Symbol $\#_{spatial}$, Offer $Value_{juice}$, Chosen Value, and Chosen Juice) constitute 14%, 28%, 17.4% and 21.7% of all task-related neurons (350), respectively (**Fig. 4b**). In the X:X task, 128 of 157 (82%) task-related responses were explained by at least 1 of the 5 variables (**Table S1**). The first three iterations of the stepwise selection procedure selected variables Chosen Quantity, Offer $Quantity_{spatial}$ and Chosen Side (**Fig. 4c**). Together, these three variables explained 98% (125/128) of the responses explained by the 5 variables (**Fig. 4c**). The best subset method selected the same three variables. Neurons encoding each of the three selected variables (Offer $Quantity_{spatial}$, Chosen Quantity and Chosen Side) constitute 29.3%, 41.4% and 8.9% of all task-related neurons (157), respectively (**Fig. 4d**).

It is intriguing that the selected variable Symbol $\#_{spatial}$ was not reported in previous studies. We postulate that it may reflect a spatial perceptual signal because it won over the confounding variable

Offer value$_{spatial}$. We further tested this hypothesis by examining the time course of encoded variables. We analyzed the activity of each cell with 100 ms time bins stepping through time with 25 ms steps. **Fig. 4e** shows the percentage of cells encoding each of the four variables at different times relative to offer presentation. The temporal profiles reveal that in the A:B task Symbol #$_{spatial}$ signal arises earlier than that of the other variables. In the X:X task, Offer Quantity$_{spatial}$ signal also seems to emerge earlier (**Fig. 4f**).

We next performed a quantitative analysis of encoding latency (EL). For each variable, we considered the time window in which a neuronal response encoded one of the variables with best fit (**Fig. 4e** and **4f**) as one instance of EL and we pooled all the time windows to generate a distribution of EL for each variable (**Fig. 4g**). We then compared the latency distribution of Symbol #$_{spatial}$ with that of other variables in the A:B task as well as the latency distribution of Offer Quanity$_{spatial}$ with that of other variables in the X:X task. In the A:B task, EL for Symbol #$_{spatial}$ (225±5.3 ms, median±ste) is significantly shorter than that for Offer Value$_{juice}$ (275±4.1 ms), Chosen Value (275±5.5 ms) as well as Chosen Juice (300±4.0 ms)($p < 0.0001$, KS tests). In the X:X task, EL for Offer Quantity (225±5.1 ms, mean±ste) is significantly shorter than that of Chosen Quantity (275.0±4.6 ms, $p < 0.0001$, KS test) but not significantly different from that of Chosen Side (250±10.1 ms, $p = 0.68$, KS test).

Separate neuronal modules represent EC and SC

Results from contrasting single neuron encoding across A:B and X:X tasks provided preliminary evidence that these two tasks may be represented by separate neuronal modules in the OFC. For a more systematic investigation, we looked at how the encoding of task-related variables remap across the two tasks. Here, the neuronal remapping across the two adjacent A:B blocks was established as the control condition and referred to as the $(A:B)_1 \rightarrow (A:B)_2$ condition while the remapping in A:B→B:B and A:B→A:A is the experimental condition and collectively referred to as A:B→X:X condition.

In total, 1078 cells were recorded under $(A:B)_1 \rightarrow (A:B)_2$ condition and 1842 cells were recorded under A:B→X:X condition. Since cross block recording stability has a significant impact on the assessment of neuronal remapping, we first verified that there is no significant difference in the stability of cross block recordings between $(A:B)_1 \rightarrow (A:B)_2$ and A:B→X:X conditions. To this end, we computed the Pearson's correlation (see **Methods**) for both the distributions of inter-spike intervals (**Fig. S1a**) and the spike waveforms (**Fig. S1b**) of the same neuron as well as the randomly paired cells across the two adjacent blocks. Based on the correlations from the test and control formulations, we computed the recording stability indices (RSI_{isi} and $RSI_{waveform}$) for each neuron (see **Methods**). Next, we assessed whether there is significant difference in RSI between $(A:B)_1 \rightarrow (A:B)_2$ and A:B→X:X conditions and the analysis yielded negative result for both the RSI_{isi} (**Fig. S1c_i and S1c_ii,** $p = 0.49$, Wilcoxon Rank-Sum Test) or $RSI_{waveform}$ (**Fig. S1c_iii and S1c_iv,** $p = 0.66$, Wilcoxon Rank-Sum Test)

To examine the remapping of cross task encoding, we first constructed a contingency table based on the result of single cell encoding in the control condition (**Fig. 5a**). The database included 281 cells that were modulated in at least one of the two blocks. We discovered that neurons tend to concentrate on either the main diagonal or the right most column and the bottom row. The interpretation of such result is that neurons encoding task-related variables in $(A:B)_1$ tend to encode the same variable or tuned out in the second block ($(A:B)_2$) of the same task. For significant tests, we first computed the odds ratio for each element of the contingency table (**Fig. 5b**). We then performed the Fisher's exact

test which assessed for each position in the contingency table, whether the cell count is deviated from the chance level, assuming that the classifications in the two trial blocks were independent. P values in **Fig. 5b** indicates whether cell counts were significantly above (red asterisks, $p < 0.05$) or below (blue asterisks, $p < 0.05$) chance. All positions on the main diagonal except for the {untuned, untuned} pair have cell counts above chance, supporting persistent coding across two blocks of the same task.

On the other hand, the contingency table (419 cells) for the experimental condition presented a very different pattern (**Fig. 5c and 5d**). Except for {Offer $\text{Quantity}_{\text{contra}}$, Symbol $\#_{\text{contra}}$}, there was no consistent mapping in the encoding of task-related variables when the animal switched from the A:B to X:X task. On the contrary, neurons encoding chosen juice in the A:B task tended to become untuned in the X:X task. Conversely, neurons encoding Chosen Quantity and Chosen Side in the X:X task tend to become untuned in the A:B task. Remarkably, neurons that are untuned in both tasks are significantly below chance, indicating complementary recruitment of neurons by each task.

Next, we directly compared the contingency tables obtained for the experimental and control conditions. We first collapsed the elements {Symbol $\#_{\text{contra}}$, Symbol $\#_{\text{contra}}$} and {Symbol $\#_{\text{ipsi}}$, Symbol $\#_{\text{ipsi}}$} in the control condition ($(A:B)_1 \rightarrow (A:B)_2$) as {Symbol #, Symbol #}. Correspondingly, we collapsed the elements {Symbol $\#_{\text{contra}}$, Offer $\text{Quantity}_{\text{contra}}$} and {Symbol $\#_{\text{ipsi}}$, Offer $\text{Quantity}_{\text{ipsi}}$} in the experimental condition (A:B→X:X) as {Symbol #, Offer Quantity}. We discovered that the odds ratio for {Symbol #, Symbol #} is significantly higher than that for {Symbol #, Offer Quantity}(**Fig. 6a**, $p < 10^{-4}$, Z test). Since previous analysis provided evidence that Symbol # coding in the A:B task reflected a spatial perceptual signal (**Fig. 4g**), a significantly lower odds ratio for {Symbol #, Offer Quantity}suggests that in the X:X task, a subset of OFC neurons encode the quantity rather than the perceptual aspect of the offers. Given the co-existence of choice outcome signal (Chosen Quantity and Chosen Side) in the X:X task (**Fig. 4g**), offer quantity information may be supplied for implementing single attribute choice in the spatial reference frame.

The results so far suggest that two modules in the OFC may be recruited to support EC and SC respectively. One module constitutes Offer Value, Chosen Value and Chosen Juice neurons while the other constitutes Offer Quantity, Chosen Quantity and Chosen Side neurons.

To further test the degree of complementarity of these two modules, we proceeded with the following analysis. For the A:B task, we collapsed variables Offer value, Chosen value and Chosen juice into variable EC, representing economic choice. Similarly, for the X:X task, we collapsed variables Offer quantity, Chosen quantity and Chosen side as SC, representing single attribute choice. We thus obtained two reduced contingency tables, one for the control condition (**Fig. 6b**), the other for the experimental condition (**Fig. 6c**). In the control condition, representation of Symbol # and EC was highly persistent across trial blocks as indicated by the observation that the cell count for {Symbol #, Symbol #} as well as {EC, EC} is significantly above chance (Symbol #: odds ratio = 12.4, $p < 10^{-6}$, Fisher's exact test; Symbol #: odds ratio = 1.73, $p < 0.05$, Fisher's exact test). Intriguingly, the contingency table for the experimental condition revealed that when the animal switched from A:B to X:X task, the probability that a EC representing neuron switches to become a SC representing neuron is significantly below chance (odds ratio = 0.40, $p < 10^{-4}$). Conversely, neurons representing EC in the A:B task tended to become untuned in the X:X task (odds ratio = 2.47, $p < 10^{-4}$, Fisher's exact test) and neurons representing SC in the X:X task tended to become untuned in the A:B task (odds ratio = 2.58, $p < 10^{-4}$, Fisher's exact test). Lastly, untuned neuronal population in each task tended to be non-

overlapping (odds ratio = 0.39, $p < 10^{-4}$, Fisher's exact test). These results indicate that there is a pattern of separate representation of EC and SC in the OFC.

To gain further insights into the representation of EC and SC during task switching, we contrasted the contingency table for the control condition (**Fig. 6b**) with that for the experimental condition (**Fig. 6c**). We compared the odds ratios of the corresponding elements in the two reduced contingency tables (**Fig. 6d ~ 6g**). Each odds ratio can be thought of as quantifying the strength of association between two particular variables across the two trial blocks. We discovered that the strength of association for $\{EC, SC\}_{A:B\rightarrow X:X}$ is significantly lower than that for $\{EC, EC\}_{(A:B)1\rightarrow(A:B)2}$ (**Fig. 6d**, $p < 10^{-4}$, Z test); the strength of association for $\{Untuned, SC\}_{A:B\rightarrow X:X}$ is significantly higher than that for $\{Untuned, EC\}_{(A:B)1\rightarrow(A:B)2}$ (**Fig. 6e**, $p < 10^{-7}$, Z test); Correspondingly, the strength of association for $\{EC, Untuned\}_{A:B\rightarrow X:X}$ is significantly higher than that for $\{EC, Untuned\}_{(A:B)1\rightarrow(A:B)2}$ (**Fig. 6f**, $p < 10^{-5}$, Z test); Lastly, the strength of association for $\{Untuned, Untuned\}_{A:B\rightarrow X:X}$ is significantly lower than that for $\{Untuned, Untuned\}_{(A:B)1\rightarrow(A:B)2}$ (**Fig. 6g**, $p < 0.01$, Z test).

Taken together, these findings implicate that EC and SC are represented by separate neuronal modules in the OFC.

Organization of functional neuronal populations in EC

The above findings suggest that EC is supported by a neuronal module separate from that representing SC. Drawing implications from neuronal organizations supporting perceptual decision making, in which sensory evidence is encoded by neuronal ensembles with organized anatomical connectivity(Albright et al., 1984; Gottlieb, 2007; Nienborg et al., 2012; Purushothaman and Bradley, 2005), we ask whether we could discover evidence supporting structured organization of value coding neurons in the OFC, where anatomical clustering of functional neuron types has rarely been reported. We are able to investigate this question thanks to the fact that in our study, most of the neurons were recorded with 16-channel linear arrays with fixed spacing (150 μm) between adjacent recording channels. We thus take the electrode spacing as the proxy of the anatomical distance between a pair of simultaneously recorded neurons.

The distance analysis was based on 419 neurons recorded across A:B and X:X tasks and that were task-related in at least one of these two tasks. Among these neurons, in the A:B task, 284 neurons provided the best fit for one of the following selected variables Symbol $\#_{spatial}$ (Symbol $\#_{contra}$ and Symbol $\#_{ipsi}$), Offer value A, Offer value B, Chosen value, Chosen juice. The pair distance analysis was focused on the neuron pairs that encoded the same variable: $\{Symbol\ \#_{contra}\}_{pair}$(14), $\{Symbol\ \#_{ipsi}\}_{pair}$(3), $\{Offer\ Value\ A\}_{pair}$(19), $\{Offer\ Value\ B\}_{pair}$(22), $\{Chosen\ Value\}_{pair}$(25), $\{Chosen\ Juice\}_{pair}$(72). To establish a null population for the A:B task, we randomly sampled the same number of neuron pairs that were not task-related in either the A:B or X:X task from the trial blocks in which at least one encoding pair was recorded. For example, if in one trial block, we identified 2 $\{Offer\ Value\ B\}_{pair}$ pairs and 3 $\{Chosen\ Juice\}_{pair}$ pairs, this trial block would contribute 5 randomly sampled Null pairs to the $\{Null_{A:B}\}$ group, which includes 155 pairs in total. In the X:X task, 125 neurons provided the best fit for one of the following selected variables $Offer\ Quantity_{spatial}$ ($Offer\ Quantity_{contra}$ and $Offer\ Quantity_{ipsi}$), Chosen Quantity, and Chosen side. Neuron pairs encoded the same variable are $\{Offer\ Quantity_{contra}\}_{pair}$(11), $\{Chosen\ Quantity\}_{pair}$(51). No neuron pair was identified for $\{Offer\ Quantity_{ipsi}\}_{pair}$ or $\{Chosen\ Side\}_{pair}$. The $\{Null_{X:X}\}$ group was formed by the same procedure as that for the $\{Null_{A:B}\}$ group.

We focused on the neuron pairs that contribute to the putative EC and SC modules. We pooled {Offer Value A}$_{pair}$, {Offer Value B}$_{pair}$, and {Chosen Value}$_{pair}$ as value coding pairs termed {Value}$_{pair}$ and {Offer Quantity$_{contra}$}$_{pair}$ and {Chosen Quantity}$_{pair}$ as quantity coding pairs termed {Quantity}$_{pair}$. For each type of coding, we also broke down the neuron pairs depending on whether the encoding slopes of the two cells have the same or opposite signs. Thus, for EC, the distance analysis included neuron pairs {Value}$_{same}$, {Value}$_{opp}$, {Chosen Juice}$_{same}$, {Chosen Juice}$_{opp}$ and {Null$_{A:B}$}, while for SC, the analysis included {Quantity}$_{same}$, {Quantity}$_{opp}$ and {Null$_{X:X}$}.

We compared the distances of neuron pairs encoding the same variable and with the same or opposite encoding signs (**Fig. 7a**). In the A:B task, distances of {Value}$_{same}$ (300$\pm$51μm, median$\pm$ste) were shorter than that for the {Value}$_{opp}$ (900$\pm$88 μm) ($p < 0.0001$, Wilcoxon Rank-Sum Test). Moreover, distances of {Value}$_{same}$ were also shorter than that of {Chosen Juice}$_{same}$ (975$\pm$101 μm, $p < 0.001$), {Chosen Juice}$_{opp}$ (600$\pm$81 μm, $p < 0.01$) and {Null$_{A:B}$} (450$\pm$40 μm, $p < 0.01$) (Wilcoxon Rank-Sum Test). In the X:X task, distances of {Quantity}$_{same}$ (600$\pm$101 μm) or {Quantity}$_{opp}$ (1050$\pm$81 μm) were not different from each other or that of {Null$_{X:X}$}(750$\pm$ 63 μm) ($p > 0.1$, Wilcoxon Rank-Sum Test). Across the A:B and X:X tasks, distances of {Value}$_{same}$ were shorter than that of{Quantity}$_{same}$ or {Quantity}$_{opp}$ ($p < 0.01$, Wilcoxon Rank-Sum Test).

The above results suggest that OFC neurons engaged in value computation and comparison in EC are anatomically clustered. We next investigated whether there is electrophysiological evidence supporting the functional organization of the value encoding neurons. As illustrated in **Fig. 6**, neurons coding task-related variables in the A:B task are mostly tuned out in the X:X task. Based on the discovery that neuronal noise correlations (rNC) are the strongest for neurons with similar tuning properties (Cohen and Newsome, 2008; Conen and Padoa-Schioppa, 2015; Liu et al., 2013; Smith and Kohn, 2008; Zohary et al., 1994), we next tested whether there was any significant change in the noise correlations among the neurons encoding the same task-related variable when the animal switched from the A:B to X:X task. Our initial analysis was focused on the pre-offer window (500 ms before offer presentation). To control for general factors that could change the neuronal noise correlations across the two tasks such as the level of arousal, we also computed the change in noise correlations for {Null$_{A:B}$} and {Null$_{X:X}$} populations as controls (see **Methods**). We discovered that when the animal switched from A:B to X:X task, comparing with the {Null$_{A:B}$} group (0.027$\pm$0.0089, median$\pm$ste), there was a significant reduction of noise correlation ($rNC_{X:X} - rNC_{A:B}$) for {Value}$_{same}$ (-0.031$\pm$0.023) (**Fig. 7b**, $p < 0.0001$, t-test), which is the group of neurons demonstrating spatial clustering. On the other hand, when switching from X:X to A:B task, there is no significant difference in the change of noise correlations ($rNC_{A:B} - rNC_{X:X}$) for {Quantity}$_{same}$ (-0.0064$\pm$0.020) or {Quantity}$_{opp}$ (0.027$\pm$0.041) comparing with that of {Null$_{X:X}$} (-0.018$\pm$0.013) (**Fig. 7c**, $p > 0.2$ t-tests).

A caveat regarding the outcome in **Fig. 7** is the potential false positive result introduced through spike sorting of neurons recorded from the same channel (pair distance = 0). In a hypothetical extreme case, during spike sorting, the spike waveforms of a neuron split into two groups may be considered two different cells. In this case, if these "two cells" encode the same value-related variable, there is a higher probability that the encoding slopes have the same rather than the opposite sign, which would erroneously boost the number of zero-distance pairs for the {Value}$_{same}$ group. To control for this scenario, we took the conservative approach removing all neuron pairs recorded from the same channel (distance = 0). We subsequently repeated the analysis performed in **Fig. 7** and the

conclusions remain unchanged (**Fig. S2**). In addition, the same noise correlation analysis performed on the post-offer window revealed a similar rNC reduction for the $\{Value\}_{same}$ group (**Fig. S3**).

The analysis so far has been focused on cell pairs encoding the same variable. As anatomical clustering and noise correlation analysis provided evidence for the organization of value coding cells, we next examined the distance and the change of rNC for two simultaneously recorded cells encoding different value-related variable pairs, namely, {Offer Value A, Offer Value B}, {Offer Value A, Chosen Value} and {Offer Value B, Chosen Value}. These cell pairs are collectively termed $\{Value_Across\}_{same}$ or $\{Value_Across\}_{opp}$ ("Across" stands for across variable) depending on whether the pair have the same or opposite sign of encoding slope. **Fig. 8a** illustrates possible types of value coding cell pairs. We compared the distances and ΔrNCs for cross-variable cell pairs with those of same-variable pairs and we made the following discoveries. First, pairwise distances for $\{Value_Within\}_{same}$ (300±51 μm, median±ste) were significantly shorter than that for $\{Value_Across\}_{same}$ (450±51 μm, $p < 0.05$, t-test) or $\{Value_Across\}_{opp}$ (600±82 μm, $p < 0.01$, t-test), meanwhile, distances for $\{Value_Within\}_{opp}$ (900±88 μm) were significantly longer than that of$\{Value_Across\}_{same}$ ($p < 0.001$, t-test) or $\{Value_Across\}_{opp}$ ($p < 0.05$, t-test) (**Fig. 8b**). Second, comparing with $\{Null_{A:B}\}$, both $\{Value_Within\}_{same}$ ($p < 0.0001$, t-test) and $\{Value_Across\}_{same}$ ($p < 0.05$, t-test) showed a significant reduction in noise correlation when the animal switched from A:B to X:X task (**Fig. 8c**). Significant noise correlation reduction was also observed for $\{Value_Within\}_{same}$ in the post-offer window (**Fig. S4**, $p < 0.01$, t-test).

To summarize, in the A:B task, neurons encoding the same value-related variables with the same sign of encoding slopes tend to form anatomical clusters and there was a significant reduction in rNC for this group of neurons when the animals switched from A:B to X:X task. These findings lend further support to the postulation that OFC harbors a specialized module for economic choice.

Discussion

We contrasted the neuronal representations under EC and SC tasks. The A:B design is an EC task that has been used in many previous studies demonstrating the abstract neuronal representation of subjective value and choice in the OFC(Cai and Padoa-Schioppa, 2014; Padoa-Schioppa, 2011; Padoa-Schioppa and Assad, 2006; Pastor-Bernier et al., 2021; Xie and Padoa-Schioppa, 2016). In contrast, in the X:X design (SC task), the animal makes a choice based on the comparison of a single attribute (i.e., juice quantity). In the A:B task, OFC neurons encoded three variables that are sufficient for generating choices in juice-based reference frame. Most of these neurons become untuned when the animal switched to the X:X task, in which a complementary set of neurons emerge to encoded offer quantity and the animal's choice in the spatial reference frame.

In the A:B task, in addition to encoding variables in juice-based reference frame, a sizeable number of neurons encoded the number of visual symbols in the spatial reference frame. Although, previous studies using the same task did not report such coding in the OFC, we speculate that symbol number coding is at least partly due to the animal's engagement in the X:X task, which elicited neuronal representation of offer quantity and quantity-based choice process in the spatial reference frame. As has been discussed in detail previously (Padoa-Schioppa and Cai, 2011), such representation may not be tied to a spatial location or a motor response per se. Moreover, the fact that in the A:B task symbol number signal emerged significantly earlier than the value signals is consistent with the

representation of bottom-up attentional signals in the OFC(McGinty, 2019; McGinty et al., 2016; Xie et al., 2018). Moreover, the strength of association for {Symbol #, Symbol #}$_{(A:B)1\rightarrow(A:B)2}$ was significantly higher than that for {Symbol #, Offer Quantity}$_{A:B\rightarrow X:X.}$ This dissociation further suggests that the representation of symbol number in the A:B task and that of offer quantity in the X:X task may serve different purposes.

A previous study showed that when switching from choice between one pair of juices (A:B) to another (C:D), the same neurons encode the same variables for the new juices, indicating a persistent choice circuit taking in different sensory inputs (Xie and Padoa-Schioppa, 2016). This result demonstrates that OFC neurons are capable of adapting their encoding identity across two blocks of trials so that the same circuit can be utilized for economic choice under different task contexts. The same implication was drawn from a recent study in which the same neural circuit seemed to support economic choices with different temporal task structures (Shi et al., 2022). Results from our current study suggest that there is likely a dedicated mapping between economic choice and the underlying neuronal circuit.

Intriguingly, in this choice circuit, the value coding neurons with the same encoding sign seem to be anatomically clustered. Since the central OFC integrates converging inputs from multiple sensory and limbic regions(Ongur and Price, 2000), the value coding clusters might emerge with developmental significance. Since connecting distant neurons requires costly wiring, clustering minimizes biologically expensive long-distance connections between these neurons (Chklovskii and Koulakov, 2004). On the other hand, the clustering observed in our study could also emerge through extensive experience of performing the juice choice task, similar to the process of the formation of category-selective regions in macaque temporal lobe in symbol training (Srihasam et al., 2012). In either case, it demonstrates that value is a prominent organization domain in the OFC. Clusters of cells selective for face were also discovered in the frontal lobe including the OFC (Rolls et al., 2006; Tsao et al., 2008). Meanwhile, it is in the OFC but not the other frontal areas that the face patches showed increased activity to expressive faces, likely reflecting the representation of value in the social domain (Azzi et al., 2012). Therefore, clustering of face selective cells in the OFC may be partially driven by value representation.

Clustering in the OFC may have significant implications for neuronal noise correlations (Shadlen and Newsome, 1998; Wimmer et al., 2015). Interestingly, we discovered that compared to that of a null population (neurons not modulated in either EC or SC), there was a significant reduction in the noise correlations among value coding neurons when the animal's engaged in the X:X rather than the A:B task. Significant noise correlations may originate from a number of sources (Kanitscheider et al., 2015), such as common input, shared connectivity (Cohen and Kohn, 2011; Shadlen and Newsome, 1998) or global fluctuations in the excitability of cortical circuits (Ecker et al., 2014; Goris et al., 2014). We postulate that the decrease of noise correlations in the X:X task might result from the fact that value coding neurons identified in the A:B task no longer integrate the information of multiple value determinants. This line of reasoning is consistent with the result in a previous study reporting the reduction in magnitude of noise correlations among vestibular nucleus neurons after the loss of convergent inputs from both the ipsilateral and contralateral otolith organs (Liu et al., 2013). Since the noise correlation reduction was in reference to the null population which were recorded simultaneously with the value coding population, we are able to control for global fluctuation of noise correlations due to factors such as the change of motivation level between the two tasks. Moreover, as the reduction of noise correlations was highly significant in the time window before the presentation

of the offers, such reduction likely reflects the difference in the functional organization of the neuronal circuit rather than being directly driven by any difference in the input between the two tasks.

With the caveat of testing the causal contribution of OFC to the X:X task, an important question is why two separate modules were recruited to support EC and SC. A few postulations are in order. First, re-structuring the choice circuit after task switch may take longer than the time span of one trial block in our experiment. Second, re-structuring circuits may be too costly. Thus, it is advantageous to maintain two separate modules configured for each task and toggle between them for optimal performance. The third and most plausible possibility is that in analogous to the face patches in the inferotemporal cortex for face processing (Tsao et al., 2006), the functional groups of neurons that have been repeatedly discovered in the OFC constitute a conserved circuit for economic choice. A working hypothesis is that such structured circuit may not only support an abstract cognitive map for flexible organization of the information of goods but also provide a possible anatomical substrate undergirding the transitivity of preferences, which is pivotal to the establishment of neoclassical economic theory (Cai, 2021; Padoa-Schioppa and Assad, 2008; Rustichini et al., 2017).

Methods

Experimental design and neuronal recordings

Two adult male rhesus monkeys (*Macaca mulatta*; monkey S, 11.4 kg; monkey N, 12.2 kg) participated in the study. All experimental procedures conformed to the NIH *Guide for the Care and Use of Laboratory Animals* and were approved by the Institutional Animal Care and Use Committee at NYU Shanghai. Before training, a head restraining device and an oval recording chamber (50 × 30 mm) were implanted on the skull under general anesthesia. The chamber was centered on stereotaxic coordinates (A30, L0) and allowed access to bilateral OFC with penetrations on a nearly coronal plane. During the experiments, monkeys sat in an electrically insulated recording room with their heads restrained. Visual stimuli were presented on a computer monitor placed 57 cm in front of the monkey. Eye positions were monitored with an infrared video camera (Eyelink, SR research). The behavioral task was controlled through custom-written software (http://www.monkeylogic.net) based on Matlab (MathWorks).

Structural MRI scans were obtained before and after the surgery. In the post-surgery MRI, a custom-made plastic insert was placed in the recording chamber with a tight fit. Cylindrical channels in the inset parallel to the path of the electrodes were filled with vitamin E oil for imaging. Coronal images were reconstructed from the MRIs to provide a reference for recording locations. Neuronal data were collected from one hemispheres of monkey S (AP 35.0mm:32.0mm, ML -4.5mm:-13.5mm, left hemisphere; anterior limit of the corpus callosum is at 31.0mm) and both hemispheres of monkey N (AP 36.0mm:33.0mm, ML-6.5mm:-11.5mm, left hemisphere; AP 35.0mm:33.0mm, ML 6.5mm:14.5mm, right hemisphere; anterior limit of the corpus callosum is at 32.0mm). Most of the recordings were performed using one or two 16-channel linear arrays (U- or V-probes; Plexon). U/V-probes had a diameter of 185 μm and contacts were 150 μm apart. The electrodes, placed ≥1 mm apart from each other, were advanced using a motorized micro-drive system (THOMAS RECORDING). A subset of data was collected using individual tungsten electrodes (125 μm diameter, Frederick Haer). Tungsten electrodes were advanced with the same micro-drive system used for linear arrays. After the electrodes reached the target sites in the OFC, we waited about 20 minutes for the tissue to settle before starting each recording session to promote signal stability. Electrical signals were recorded using a 32-channel system (Plexon Inc). Action potentials were detected online and saved to disk for

spike sorting using standard software (Offline Sorter, Plexon Inc). Only neurons that remained stable and well-isolated during two consecutive trial blocks were included in the analysis.

Fig. 1a illustrates the experimental design. In each trial, the animal chose between two juices offered in variable amounts. The trial began with the monkey gazing a fixation point in the center of the monitor (center fixation window: 3°). After 0.5 s, two sets of squares representing the two offers appeared on the two sides of the fixation point. For each offer, the color indicated the juice type and the number of squares indicated juice quantity, with each square representing a juice quantum 100 µl). The animal maintained center fixation for a randomly variable delay (0.6–1.2 s, uniform distribution) followed by a go signal, which was indicated by the extinction of the center fixation point and the appearance of two saccade targets. The monkey had 1.5 s to indicate its choice with a saccade and was required to maintain target fixation (peripheral fixation window: 4°) for 0.3 s before juice delivery.

In our study, A:B indicates choice between two juices with A as the one with the preferred taste; B:B or A:A indicates choice between the same juice. The same two juices were used in each session. Since each session included two A:B blocks, they are named in their temporal sequence in the experimental session. For monkey S, the block sequence is B:B, $(A:B)_1$, $(A:B)_2$, A:A; For monkey N, the block sequence is B:B, $(A:B)_1$, $(A:B)_2$, A:A or $(A:B)_1$, $(A:B)_2$, A:A, $(A:B)_3$. For the purpose of cross task comparison, we ensured the stability of recording in adjacent recording blocks. Based on our design, $(A:B)_1 \rightarrow (A:B)_2$ serves as the control condition while $(A:B)_1 \rightarrow$ B:B and $(A:B)_2 \rightarrow$ A:A serve as the contrast for neuronal representation in economic choice and single-attribute choice and are collectively termed A:B→X:X.

The offer combinations for the A:B blocks arranged in descending order of the (A/B) quantity ratio is: [1A:0B 3A:1B 2A:1B 2A:2B 1A:2B 1A:3B 1A:4B 1A:6B 0A:2B]; For the purpose of performing the matching analysis as that for the A:B block, in B:B block, in which the same juice was used, one of the two offers was coded as lowercase “a”. Thus, the offer combination for B:B blocks was coded as [2a:0B 6a:1B 4a:1B 3a:1B 2a:1B 2a:2B 1a:2B 1a:3B 1a:4B 1a:6B 0a:2B]. By the same token, the offer combination in the A:A block was coded as: [2A:0b 3A:1b 2A:1b 1A:1b 1A:2b 1A:3b 0A:2b]. The offer combinations for B:B and A:A blocks are designed such that the value range for offer A and offer B remains the same as that in the A:B block. For the A:B task, a "trial type" was defined by two offers and a choice (e.g., [1A+:3B-, A]). In this notation, "+" indicates offer locating on the left hemifield while "-" indicates offer locating on the right hemifield. For the B:B or A:A task, because therefore is only one type of juice and the animals almost always choose the larger quantity offer, “trial type” was defined by two offers and the location of the larger quantity offer (e.g., [1B+:3B-]).

Blinding was not used in the behavioral design. In each block, offer types were pseudo-randomly interleaved and the left/right configurations of the offers were counterbalanced. In all sessions, the two blocks were separated by a ~5 min break. The number of cells collected for each condition and the number of trials run for each cell were not predetermined using a statistical method, but were comparable to those of previous studies.

Behavioral analysis and neuronal classification

Behavioral data were analyzed separately for each trial block. The 'choice pattern' was defined as the percent of trials in which the animal chose the non-preferred juice as a function of the log quantity ratio of the two offers. In the analysis, we fitted the choice pattern with a normal cumulative

distribution function. The flex of the sigmoid, corresponding to the indifference point (ρ), provided a measure for the relative value between the two offers.

The analysis performed for each cell in each trial block followed the procedures used in previous studies. Neuronal activity was examined in two time windows: pre-offer (0.5 s before offer), and post-offer (0.1~0.6 s after the offer) window. Firing rates were obtained by averaging spike counts over each time window and across trials for each trial type. A 'neuronal response' was defined as the firing rate of one cell, in one block, in one time window, as a function of trial type. The two responses recorded for the same cell, in the same time window, in the adjacent two blocks is defined as a 'response pair'. For each neuron and each time window, we performed a one-way ANOVA (factor: trial type) separately in each block. We imposed a $p < 0.01$ threshold and admitted to subsequent analyses only response pairs that met this criterion in at least one block. Neurons that passed this ANOVA criterion in at least one time window were identified as 'task-related'.

Data from each trial block were considered separately. The entire data set for the A:B task included 2,029 cells. Previous work showed that the vast majority of neuronal responses encoded one of three variables: Offer Value, Chosen Value and Chosen Juice. For each variable, the encoding was linear and either positive (increasing firing rate for increasing values) or negative (increasing firing rate for decreasing values). Thus, as a preliminary step, we repeated the variable selection analyses conducted previously on the current data set in the A:B task. We computed 11 variables (Table S1) and applied the stepwise and best-subset procedures for variable selection. A variable was said to 'explain' the response if the regression slope differed significantly from zero ($p < 0.05$). The regression also provided an R^2, which was set equal to zero if the variable did not explain the response. The variable with the highest R^2 is assigned to the cell as the encoded variable. Both procedures selected variables Symbol $\#_{spatial}$, Offer $value_{juice}$, Chosen Value and Chosen Juice. The same analysis was applied to the X:X task (1,964 cells) with another set of variables potentially encoded (Table S1) and the selected variables are Offer $Quantity_{spatial}$, Chosen Quantity and Chosen Side.

Comparing neuronal classifications across tasks

To compare the classifications across trial blocks at the population level, we constructed contingency tables separately for data collected in $(A:B)_1 \rightarrow (A:B)_2$ condition and A:B→X:X condition. The rows and columns of the tables represent the classifications of neurons in the two blocks respectively, while the numbers represent cell counts. Our initial analysis was to assess, for each location in the contingency table, whether the cell count deviated significantly from chance level, assuming independent classifications in the two trial blocks. To this end, we used the statistical test based on odds ratio.

We indicate with $X_{i,j}$ the number of cells encoding variable i in the first block and variable j in the second block. For each location (i, j) in the table, we computed a 2 × 2 matrix with elements

$$a_{11} = X_{i,j}, a_{12} = \sum_{n \neq j} X_{i,n}\ , a_{21} = \sum_{m \neq i} X_{m,j}\ \ and\ a_{22} = \sum\nolimits_{n \neq j, m \neq i} X_{m,n}$$

The odds ratio for location (i, j) was defined as $OR_{i,j} = (a_{11}/a_{12})/(a_{21}/a_{22})$. If the likelihood of a neuron encoding variable i in the first block is independent of the likelihood of it encoding variable j in the second block, the expected value of $OR_{i,j}$ equals 1. In other words, the chance level for odds ratio is 1.

Conversely, $OR_{i,j} > 1$ ($OR_{i,j} < 1$) indicated that the cell count in location (i, j) was above (below) chance level. To assess whether departures from chance level were statistically significant, we used Fisher's exact test (two tails).

Comparing the remapping across the control and experimental condition

In a series of analyses, we directly compared the classification results obtained for the control ($(A:B)_1 \rightarrow (A:B)_2$) and experimental ($A:B \rightarrow X:X$) conditions. For each condition, we constructed a reduced contingency table. We then constructed 2 × 2 contingency tables for the elements of interest. Finally, we compared the odds ratios associated with each corresponding pair of elements with a Z-test.

Verification of recording stability across trial blocks

The validity of comparison of cross block representations for $(A:B)_1 \rightarrow (A:B)_2$ and $A:B \rightarrow X:X$ conditions is contingent upon the assumption that recording was stable across two trial blocks and there is no significant difference between the stability of recording across the above two conditions.

To test this assumption, we computed the Pearson correlation for both the distribution of inter-spike intervals (CC_{isi_same}) and the spike waveforms ($CC_{waveform_same}$) of the same neuron across the two adjacent blocks. We also constructed a dataset of control distribution as CC_{isi_random} and $CC_{waveform_random}$ by pairing a neuron in one block with a randomly selected different neuron in the next block. Finally, we computed the difference of the Pearson correlation between the experiment and control condition as the recording stability index (RSI) based on inter-spike intervals and the spike waveforms as follows.

$$RSI_{isi} = (CC_{isi_same} - CC_{isi_random})/(CC_{isi_same} + CC_{isi_random})$$
$$RSI_{waveform} = (CC_{waveform_same} - CC_{waveform_random})/(CC_{waveform_same} + CC_{waveform_random})$$

Lastly, we compared the RSI_{isi} and $RSI_{waveform}$ between $(A:B)_1 \rightarrow (A:B)_2$ and $A:B \rightarrow X:X$ conditions using the Wilcoxon Rank-Sum Test.

Analysis of neuron pair distance

In our study, most of the neurons were recorded with 16-channel linear arrays with known spacing (150 μm) between adjacent recording channels. We thus take the electrode channel spacing as the proxy of the anatomical distance between a pair of simultaneously recorded neurons. If a pair of neurons were recorded from same channel, their distance was considered zero.

Analysis of noise correlations

Noise correlation (rNC) was defined as Pearson's correlation between the trial-to-trial activity of two simultaneously recorded neurons. For each cell, each trial type, we computed the mean firing rate and SD across trials in the pre-offer and post-offer time window separately. We z-scored the firing rate in each trial accordingly and obtained a normalized activity. We then computed Pearson's correlation (ρ) between normalized activity fluctuations for each trial type in the two time windows for simultaneously recorded cells. The pairwise rNC for each time window is the averaged ρ across trial types.

Reference

Albright, T.D., Desimone, R., and Gross, C.G. (1984). Columnar organization of directionally selective cells in visual area MT of the macaque. J Neurophysiol *51*, 16-31.

Azzi, J.C., Sirigu, A., and Duhamel, J.R. (2012). Modulation of value representation by social context in the primate orbitofrontal cortex. Proc Natl Acad Sci U S A *109*, 2126-2131.

Behrens, T.E.J., Muller, T.H., Whittington, J.C.R., Mark, S., Baram, A.B., Stachenfeld, K.L., and Kurth-Nelson, Z. (2018). What Is a Cognitive Map? Organizing Knowledge for Flexible Behavior. Neuron *100*, 490-509.

Benedek, M., Jauk, E., Sommer, M., Arendasy, M., and Neubauer, A.C. (2014). Intelligence, creativity, and cognitive control: The common and differential involvement of executive functions in intelligence and creativity. Intelligence *46*, 73-83.

Cai, X. (2021). The Neural Instantiation of an Abstract Cognitive Map for Economic Choice. Neuroscience *477*, 106-114.

Cai, X., and Padoa-Schioppa, C. (2014). Contributions of orbitofrontal and lateral prefrontal cortices to economic choice and the good-to-action transformation. Neuron *81*, 1140-1151.

Cai, X., and Padoa-Schioppa, C. (2019). Neuronal evidence for good-based economic decisions under variable action costs. Nat Commun *10*, 393.

Chklovskii, D.B., and Koulakov, A.A. (2004). Maps in the brain: what can we learn from them? Annu Rev Neurosci *27*, 369-392.

Cohen, M.R., and Kohn, A. (2011). Measuring and interpreting neuronal correlations. Nat Neurosci *14*, 811-819.

Cohen, M.R., and Newsome, W.T. (2008). Context-dependent changes in functional circuitry in visual area MT. Neuron *60*, 162-173.

Conen, K.E., and Padoa-Schioppa, C. (2015). Neuronal variability in orbitofrontal cortex during economic decisions. J Neurophysiol *114*, 1367-1381.

Conen, K.E., and Padoa-Schioppa, C. (2019). Partial Adaptation to the Value Range in the Macaque Orbitofrontal Cortex. J Neurosci *39*, 3498-3513.

Connolly, J.D., Andersen, R.A., and Goodale, M.A. (2003). FMRI evidence for a 'parietal reach region' in the human brain. Exp Brain Res *153*, 140-145.

Conway, B.R., Moeller, S., and Tsao, D.Y. (2007). Specialized color modules in macaque extrastriate cortex. Neuron *56*, 560-573.

Downing, P.E., Jiang, Y., Shuman, M., and Kanwisher, N. (2001). A cortical area selective for visual processing of the human body. Science *293*, 2470-2473.

Ecker, A.S., Berens, P., Cotton, R.J., Subramaniyan, M., Denfield, G.H., Cadwell, C.R., Smirnakis, S.M., Bethge, M., and Tolias, A.S. (2014). State dependence of noise correlations in macaque primary visual cortex. Neuron *82*, 235-248.

Gavrilov, N., Hage, S.R., and Nieder, A. (2017). Functional Specialization of the Primate Frontal Lobe during Cognitive Control of Vocalizations. Cell reports *21*, 2393-2406.

Goris, R.L., Movshon, J.A., and Simoncelli, E.P. (2014). Partitioning neuronal variability. Nat Neurosci *17*, 858-865.

Gottlieb, J. (2007). From thought to action: the parietal cortex as a bridge between perception, action, and cognition. Neuron *53*, 9-16.

Kanitscheider, I., Coen-Cagli, R., and Pouget, A. (2015). Origin of information-limiting noise correlations. Proc Natl Acad Sci U S A *112*, E6973-6982.

Kanwisher, N. (2010). Functional specificity in the human brain: a window into the functional architecture of the mind. Proc Natl Acad Sci U S A *107*, 11163-11170.

Kanwisher, N., McDermott, J., and Chun, M.M. (1997). The fusiform face area: a module in human extrastriate cortex specialized for face perception. J Neurosci *17*, 4302-4311.

Kobayashi, S., Pinto de Carvalho, O., and Schultz, W. (2010). Adaptation of reward sensitivity in orbitofrontal neurons. J Neurosci *30*, 534-544.

Liu, S., Dickman, J.D., Newlands, S.D., DeAngelis, G.C., and Angelaki, D.E. (2013). Reduced choice-related activity and correlated noise accompany perceptual deficits following unilateral vestibular lesion. Proc Natl Acad Sci U S A *110*, 17999-18004.

McGinty, V.B. (2019). Overt Attention toward Appetitive Cues Enhances Their Subjective Value, Independent of Orbitofrontal Cortex Activity. eNeuro *6*.

McGinty, V.B., Rangel, A., and Newsome, W.T. (2016). Orbitofrontal Cortex Value Signals Depend on Fixation Location during Free Viewing. Neuron *90*, 1299-1311.

Nienborg, H., Cohen, M.R., and Cumming, B.G. (2012). Decision-related activity in sensory neurons: correlations among neurons and with behavior. Annu Rev Neurosci *35*, 463-483.

O'Reilly, R.C. (2010). The What and How of prefrontal cortical organization. Trends in Neurosciences *33*, 355-361.

Ongur, D., and Price, J.L. (2000). The organization of networks within the orbital and medial prefrontal cortex of rats, monkeys and humans. Cereb Cortex *10*, 206-219.

Padoa-Schioppa, C. (2009). Range-adapting representation of economic value in the orbitofrontal cortex. J Neurosci *29*, 14004-14014.

Padoa-Schioppa, C. (2011). Neurobiology of economic choice: a good-based model. Annu Rev Neurosci *34*, 333-359.

Padoa-Schioppa, C., and Assad, J.A. (2006). Neurons in orbitofrontal cortex encode economic value. Nature *441*, 223-226.

Padoa-Schioppa, C., and Assad, J.A. (2008). The representation of economic value in the orbitofrontal cortex is invariant for changes of menu. Nat Neurosci *11*, 95-102.

Padoa-Schioppa, C., and Cai, X. (2011). The orbitofrontal cortex and the computation of subjective value: consolidated concepts and new perspectives. Ann N Y Acad Sci *1239*, 130-137.

Pastor-Bernier, A., Stasiak, A., and Schultz, W. (2021). Reward-specific satiety affects subjective value signals in orbitofrontal cortex during multicomponent economic choice. Proc Natl Acad Sci U S A *118*.

Purushothaman, G., and Bradley, D.C. (2005). Neural population code for fine perceptual decisions in area MT. Nat Neurosci *8*, 99-106.

Riley, M.R., Qi, X.L., and Constantinidis, C. (2017). Functional specialization of areas along the anterior-posterior axis of the primate prefrontal cortex. Cereb Cortex *27*, 3683-3697.

Rolls, E.T., Critchley, H.D., Browning, A.S., and Inoue, K. (2006). Face-selective and auditory neurons in the primate orbitofrontal cortex. Exp Brain Res *170*, 74-87.

Rustichini, A., Conen, K.E., Cai, X., and Padoa-Schioppa, C. (2017). Optimal coding and neuronal adaptation in economic decisions. Nat Commun *8*, 1208.

Salthouse, T.A., Fristoe, N., McGuthry, K.E., and Hambrick, D.Z. (1998). Relation of task switching to speed, age, and fluid intelligence. Psychol Aging *13*, 445-461.

Shadlen, M.N., and Newsome, W.T. (1998). The variable discharge of cortical neurons: implications for connectivity, computation, and information coding. J Neurosci *18*, 3870-3896.

Shi, W., Ballesta, S., and Padoa-Schioppa, C. (2022). Economic Choices under Simultaneous or Sequential Offers Rely on the Same Neural Circuit. J Neurosci *42*, 33-43.

Smith, M.A., and Kohn, A. (2008). Spatial and temporal scales of neuronal correlation in primary visual cortex. J Neurosci *28*, 12591-12603.

Srihasam, K., Mandeville, J.B., Morocz, I.A., Sullivan, K.J., and Livingstone, M.S. (2012). Behavioral and anatomical consequences of early versus late symbol training in macaques. Neuron *73*, 608-619.

Tremblay, L., and Schultz, W. (1999). Relative reward preference in primate orbitofrontal cortex. Nature *398*, 704-708.

Tsao, D.Y., Freiwald, W.A., Tootell, R.B., and Livingstone, M.S. (2006). A cortical region consisting entirely of face-selective cells. Science *311*, 670-674.

Tsao, D.Y., Schweers, N., Moeller, S., and Freiwald, W.A. (2008). Patches of face-selective cortex in the macaque frontal lobe. Nat Neurosci *11*, 877-879.

Wimmer, K., Compte, A., Roxin, A., Peixoto, D., Renart, A., and de la Rocha, J. (2015). Sensory integration dynamics in a hierarchical network explains choice probabilities in cortical area MT. Nat Commun *6*, 6177.

Xie, J., and Padoa-Schioppa, C. (2016). Neuronal remapping and circuit persistence in economic decisions. Nat Neurosci *19*, 855-861.

Xie, Y., Nie, C., and Yang, T. (2018). Covert shift of attention modulates the value encoding in the orbitofrontal cortex. eLife *7*.

Yang, G.R., Cole, M.W., and Rajan, K. (2019a). How to study the neural mechanisms of multiple tasks. Curr Opin Behav Sci *29*, 134-143.

Yang, G.R., Joglekar, M.R., Song, H.F., Newsome, W.T., and Wang, X.J. (2019b). Task representations in neural networks trained to perform many cognitive tasks. Nat Neurosci *22*, 297-306.

Zeki, S.M. (1978). Functional specialisation in the visual cortex of the rhesus monkey. Nature *274*, 423-428.

Zohary, E., Shadlen, M.N., and Newsome, W.T. (1994). Correlated neuronal discharge rate and its implications for psychophysical performance. Nature *370*, 140-143.

A:B	Collapsed variable	Variable	Definition	Reference frame
1	Offer Value (juice)	Offer Value A	ρq_A	Juice
2		Offer Value B	q_B	Juice
3		Chosen Juice	1 if juice B is chosen, 0 if juice A is chosen	Juice
4		Chosen Value	offer value A if juice A chosen, offer value B if juice B chosen	
5		Other Value	offer value B if juice A chosen, offer value A if juice B chosen	
6	Offer Value (spatial)	Offer $\text{Value}_{\text{contra}}$	offer value A/offer value B if offer A/offer B is on the contralateral hemifield	Action
7		Offer $\text{Value}_{\text{ipsi}}$	offer value A/offer value B if offer A/offer B is on the ipsilateral hemifield	Action
8		Chosen Side	1 if contralateral offer is chosen, 0 if ipsilateral offer is chosen	Action
9	Symbol # (spatial)	Symbol $\#_{\text{contra}}$	number of squares associated with the offer in the contralateral hemifield	Visual
10		Symbol $\#_{\text{ipsi}}$	number of squares associated with the offer in the ipsilateral hemifield	Visual
11		Position of A	1 if offer A is on the contralateral hemifield, 0 if offer A is on the ipsilateral hemifield	
X:X				
1	Offer Quantity (spatial)	Offer $\text{Quantity}_{\text{contra}}$	quantity of the juice offered on the contralateral hemifield	Action
2		Offer $\text{Quantity}_{\text{ipsi}}$	quantity of the juice offered on the ipsilateral hemifield	Action
3		Chosen Side	1 if contralateral offer is chosen, 0 if ipsilateral offer is chosen	Action
4		Chosen Quantity	quantity of the chosen offer	
5		Other Quantity	quantity of the unchosen offer	

Table S1. Defined variables. For the A:B task, in any given trial, q_A and q_B were, respectively, the quantities of juice A and juice B offered to the animal, ρ was the relative value of the two juices obtained from a sigmoid fit.

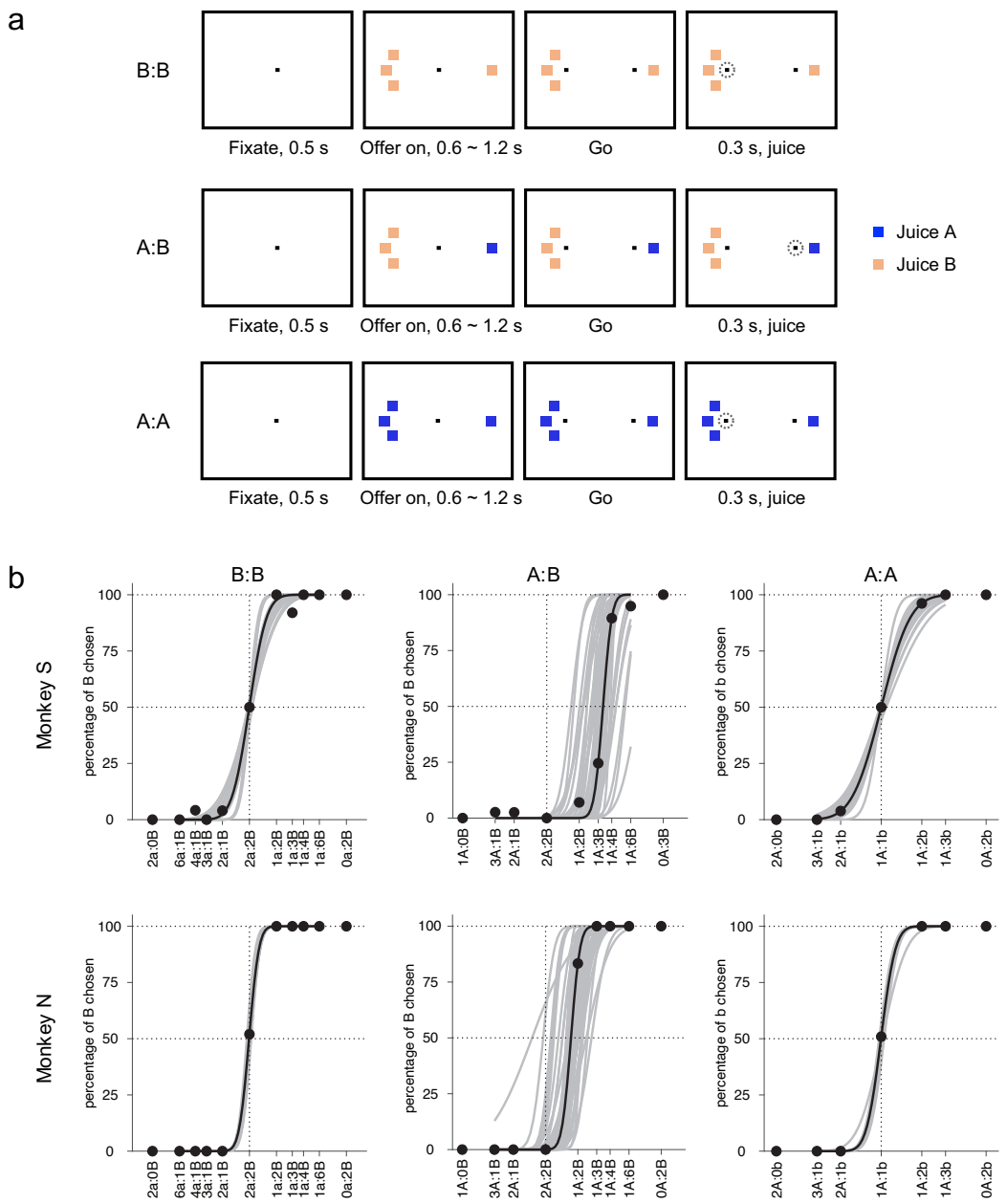

Figure 1. Experimental design and behavioral analysis. (**a**) The same two juices (A and B) were used in one experimental session with juice A the preferred one. One experimental session typically includes 4 blocks of trials in the sequence of B:B, A:B, A:B and A:A. The temporal structure of the task is the same for all blocks. (**b**) Choice patterns, all sessions. For the purpose of performing a matching analysis as that for the A:B blocks, in B:B blocks, one of the two offers was coded as lowercase 'a' and in A:A blocks, one of the two offers was coded as lowercase 'b'. Each gray line indicates the sigmoid fit for one block of trials. The black dots and the black line of sigmoid fit are based on the trial block with the median ρ value among all blocks.

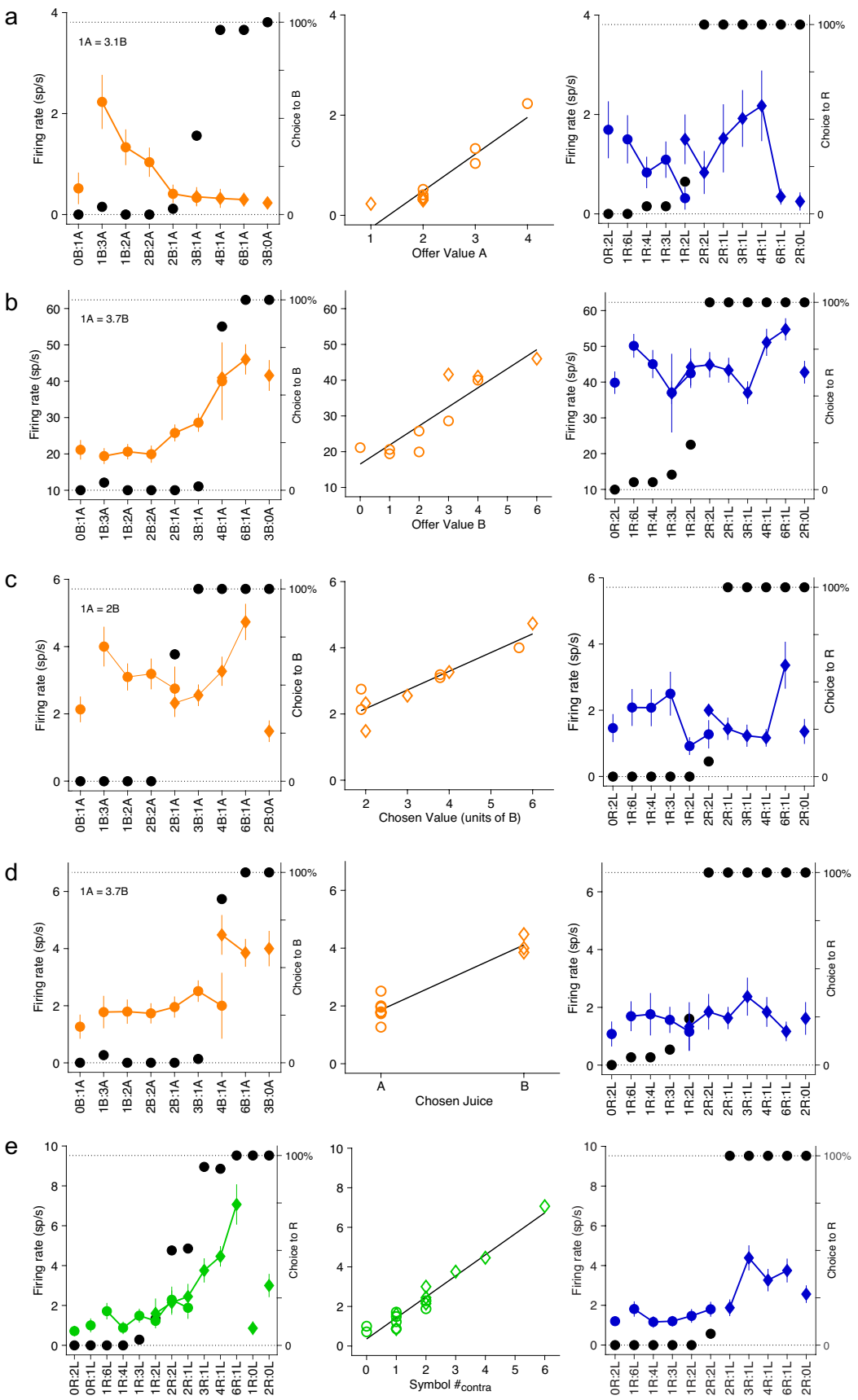

Figure 2. Example neurons encoding task-related variables in EC. In **a-d**, the left panel shows the activity of the cell recorded in the A:B task; The x axis represents different offer types ranked by ratio

#B:#A. Black symbols represent the percentage of ‘‘B’’ choices. Orange symbols represent the neuronal firing rate (circles and diamonds for choices of juice A and juice B). In **e**, the left panel shows the activity of the cell recorded in the A:B task; The x axis represents different offer types ranked by ratio #R:#L. Black symbols represent the percentage of ‘‘R’’ choices. Green symbols represent the neuronal firing rate (circles and diamonds stand for choices to the left and right). In all figures, the middle panel shows the activity of the neuron plotted against the encoded variable; The black line is derived from a linear regression. The right panel shows the activity of the same cell but recorded in the adjacent B:B block. The x axis represents different reward quantity combinations ranked by ratio #R:#L. Black symbols represent the percentage of ‘‘R’’ choices. Blue symbols represent the neuronal firing rate (circles and diamonds for choices to the left and right). (**a**) Cell encoding Offer Value A ($R^2 = 0.88$, $p < 10^{-4}$). This cell did not encode any defined task-related variables (Table S1) in the B:B task. (**b**) Cell encoding Offer Value B ($R^2 = 0.80$, $p < 10^{-3}$). This cell encoded Chosen Quantity in the B:B task ($R^2 = 0.37$, $p < 0.05$). (**c**) Cell encoding Chosen Value ($R^2 = 0.86$, $p < 10^{-3}$). This cell did not encode any defined task-related variables in the B:B task. (**d**) Cell encoding Chosen Juice ($R^2 = 0.91$, $p < 10^{-4}$). This cell did not encode any defined task-related variables in the B:B task. (**e**) Cell encoding Symbol $\#_{contra}$ ($R^2 = 0.94$, $p < 10^{-9}$). This cell encoded Offer $Quantity_{contra}$ in the B:B task ($R^2 = 0.57$, $p < 0.05$). Firing rates shown here are from the post-offer time window. For these neurons, the numbers of trials in the A:B and B:B block were as follows: (**a**) 269, 265, (**b**) 290, 284, (**c**) 308, 273, (**d**) 290, 284, (**e**) 285, 342.

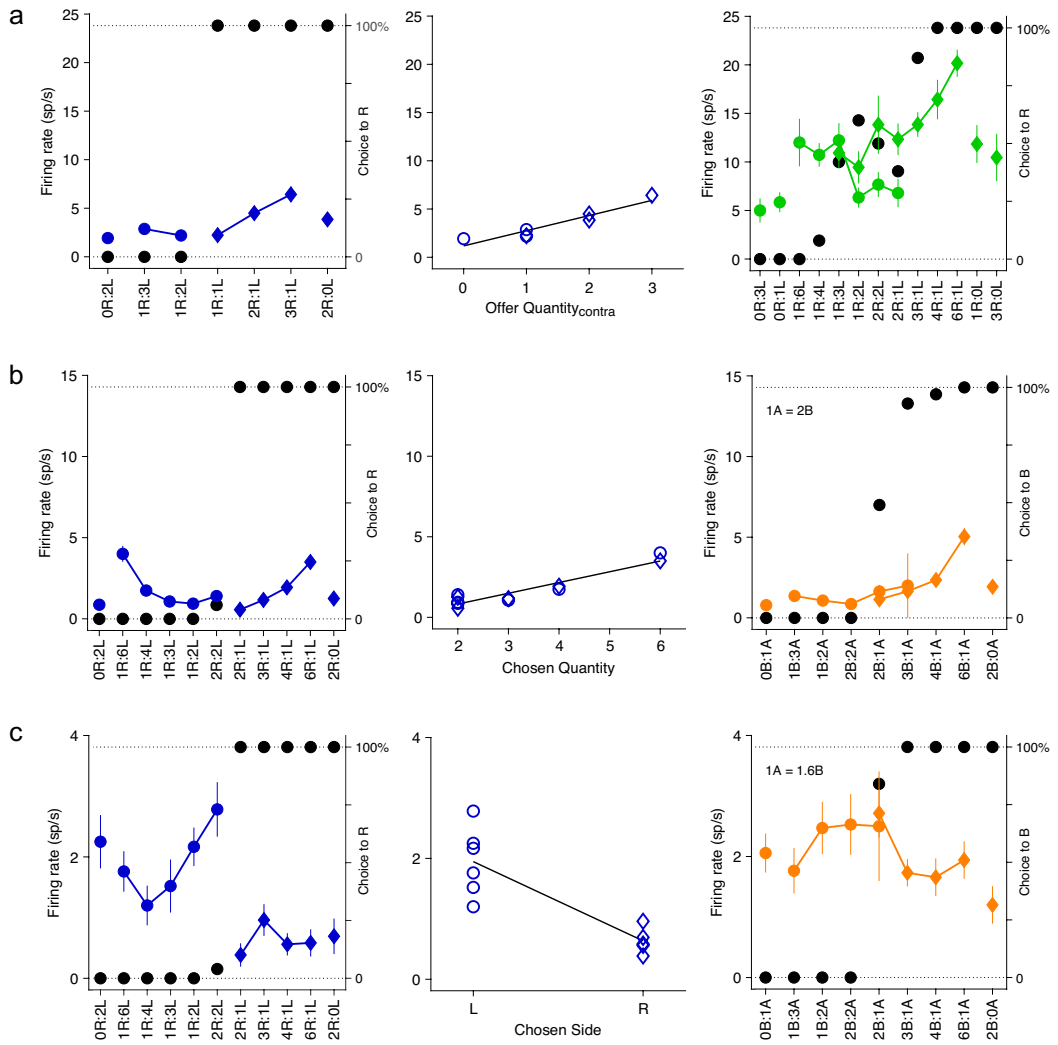

Figure 3. Example neurons encoding task-related variables in the SC. The left panel shows the activity of the cell recorded in the A:A or B:B block; The x axis represents different reward quantity combinations ranked by ratio #R:#L; Black symbols represent the percentage of ''R'' choices; Blue symbols represent the neuronal firing rate (circles and diamonds for choices to the left and right). The middle panel shows the activity of the neuron plotted against the encoded variable; The black line is derived from a linear regression. The right panel shows the activity of the cell recorded in the adjacent A:B block of the same session. The x axis represents different offer types ranked by ratio #B:#A. Black symbols represent the percentage of ''B'' choices. Orange symbols represent the neuronal firing rate (circles and diamonds for choices of juice A and juice B). (**a**) Cell encoding Offer Quantity$_{contra}$ ($R^2 = 0.89$, $p < 0.01$). This cell encoded Symbol #$_{contra}$ in the A:B task ($R^2 = 0.40$, $p < 0.05$). (**b**) Cell encoding Chosen Quantity ($R^2 = 0.89$, $p < 10^{-4}$). This cell did not encode any defined task-related variables in the A:B task (Table S1). (**c**) Cell encoding Chosen Side ($R^2 = 0.72$, $p < 10^{-3}$). This cell did not encode any defined task-related variables in the A:B task. Firing rates shown here are from the post-offer time window. For these neurons, the numbers of trials in each trial block were as follows: (**a**) 342, 266, (**b**) 369, 249, (**c**) 273, 266.

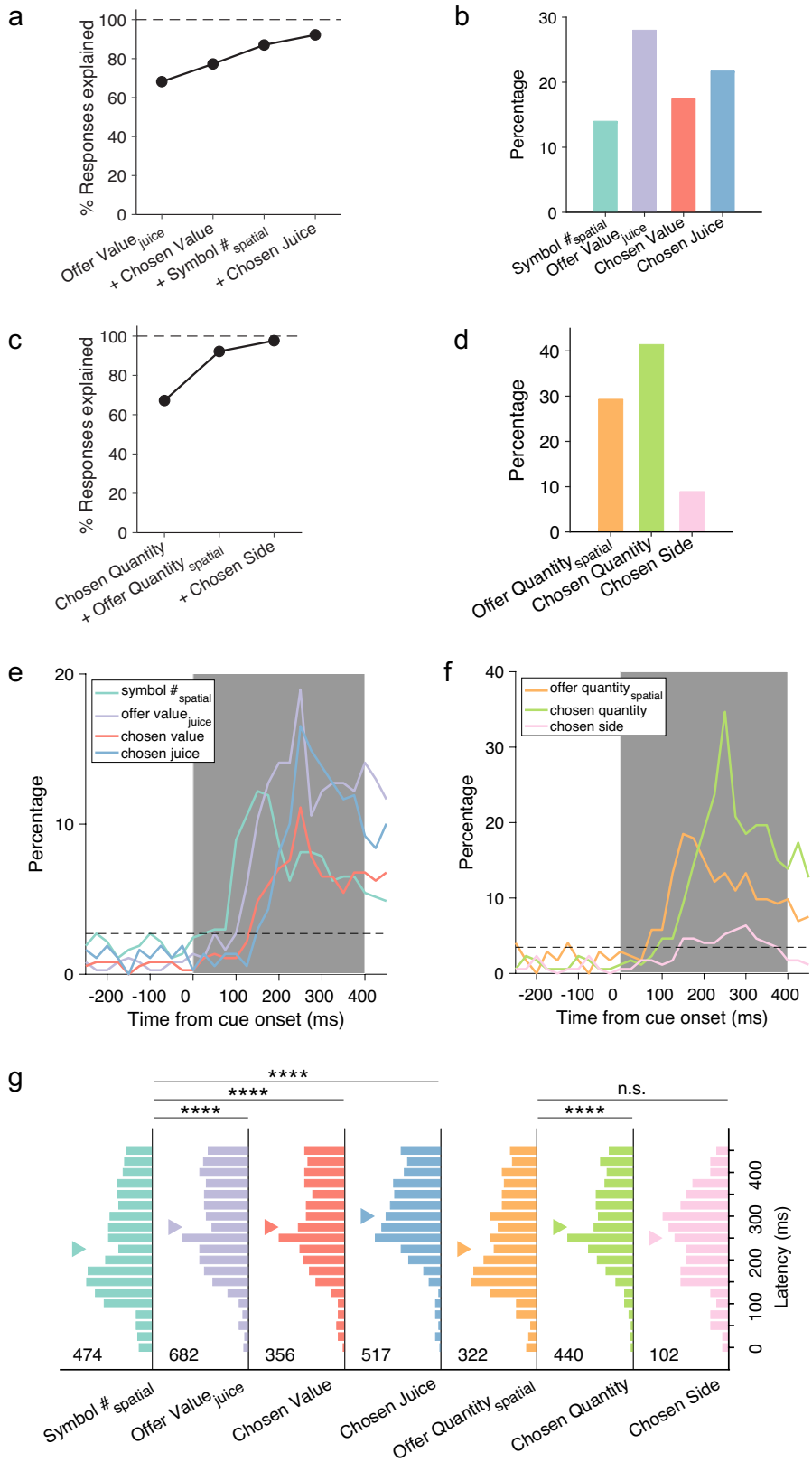

Figure 4. Encoding of task-related variables. (**a**) Stepwise selection, percentage of explained responses. The figure illustrates the percentage of responses explained at subsequent iterations of the stepwise procedure ("+" on the abscissa indicates inclusion of the variable. In this plot, the "100" dotted line represents the total number of responses explained overall by the 11 variables examined for the A:B task (Table S1). The four variables Offer Value$_{juice}$, Chosen Value, Symbol #$_{spatial}$ and Chosen Juice collectively explained 92% of the responses explained by the 11 variables.

(**b**) Percentage of neurons encoding each selected variable in the A:B task. (**c**) Same as in (**a**) but for X:X task. The three variables Chosen Quantity, Offer $\text{Quantity}_{\text{spatial}}$ and Chosen Side explained 98% of the responses explained by the 5 variables examined for the X:X task (Table S1). (**d**) Percentage of neurons encoding each selected variable in the X:X task. (**e**) Time course of percentage of encoded variables in the A:B task. Dotted horizontal line indicates the percentage significantly above the chance level of 1% (binomial test, $p < 0.05$). Solid vertical line indicates time of offer on. (**f**) Same as in (**e**) but for the encoded variables in X:X task. (**g**) Distribution of encoding latency for encoded variables in A:B and X:X task. Number in each subplot indicates the number of responses encoding the corresponding variable. Difference in latency distribution between Symbol $\#_{\text{spatial}}$ and other variables in the A:B task was tested using the Kolmogorov–Smirnov test (****$p < 0.0001$); Difference in encoding latency distribution between Offer $\text{Quantity}_{\text{spatial}}$ and other variables in the X:X task was tested using the same test (****$p < 0.0001$; n.s., not significant).

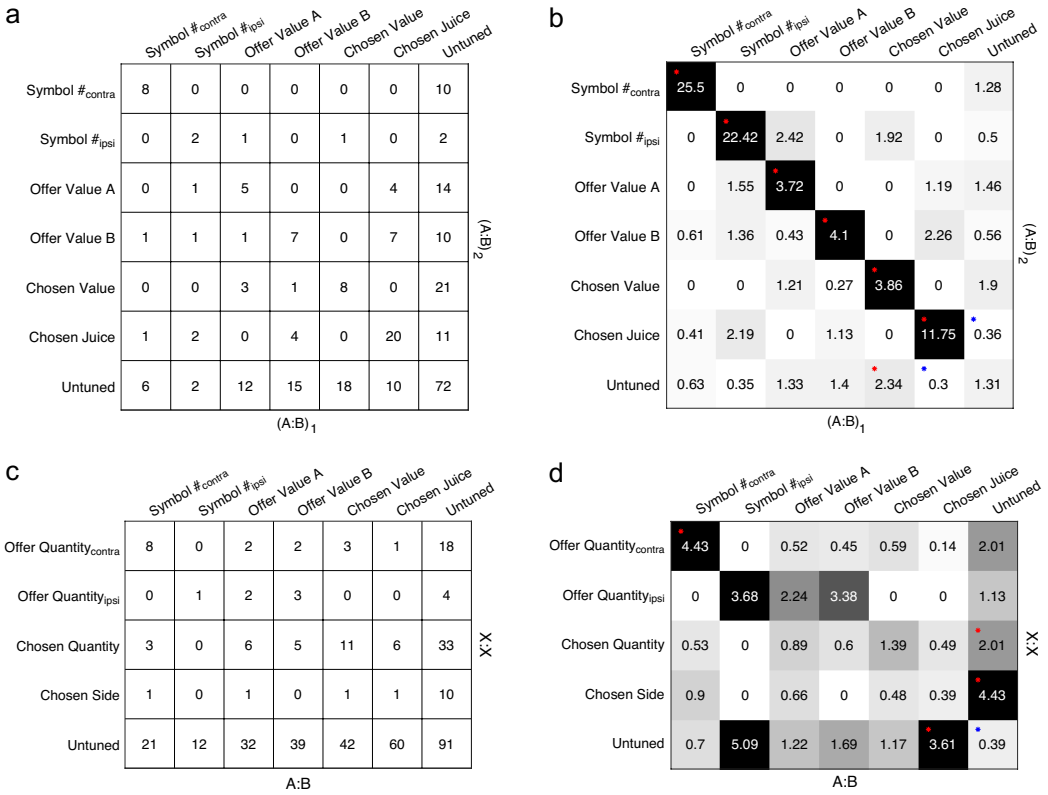

Figure 5. Contrasting classifications across trial blocks. This population analysis was conducted separately for $(A:B)_1 \rightarrow (A:B)_2$ (**a** and **b**) and A:B→X:X (**c** and **d**). (**a**) Contingency table, $(A:B)_1 \rightarrow (A:B)_2$ ($n = 281$). Rows and columns represent, respectively, the classification obtained in the first and the second A:B block. Numbers in the table indicate cell counts. Task-related cells not explained by any variable were classified as untuned. (**b**) Analysis of odds ratios, $(A:B)_1 \rightarrow (A:B)_2$. Numbers in the table and grayscale colors represent the odds ratios obtained for each location in (**a**). Chance level is 1 and numbers >1 (or <1) indicate that the cell count was above (or below) that expected by chance. For each location, we performed Fisher's exact test. Red asterisks indicate that the cell count was significantly above chance ($p < 0.05$) while blue asterisks indicate that the cell count was significantly below chance ($p < 0.05$). (**c** and **d**) Same as (**a** and **b**) but for A:B→X:X.

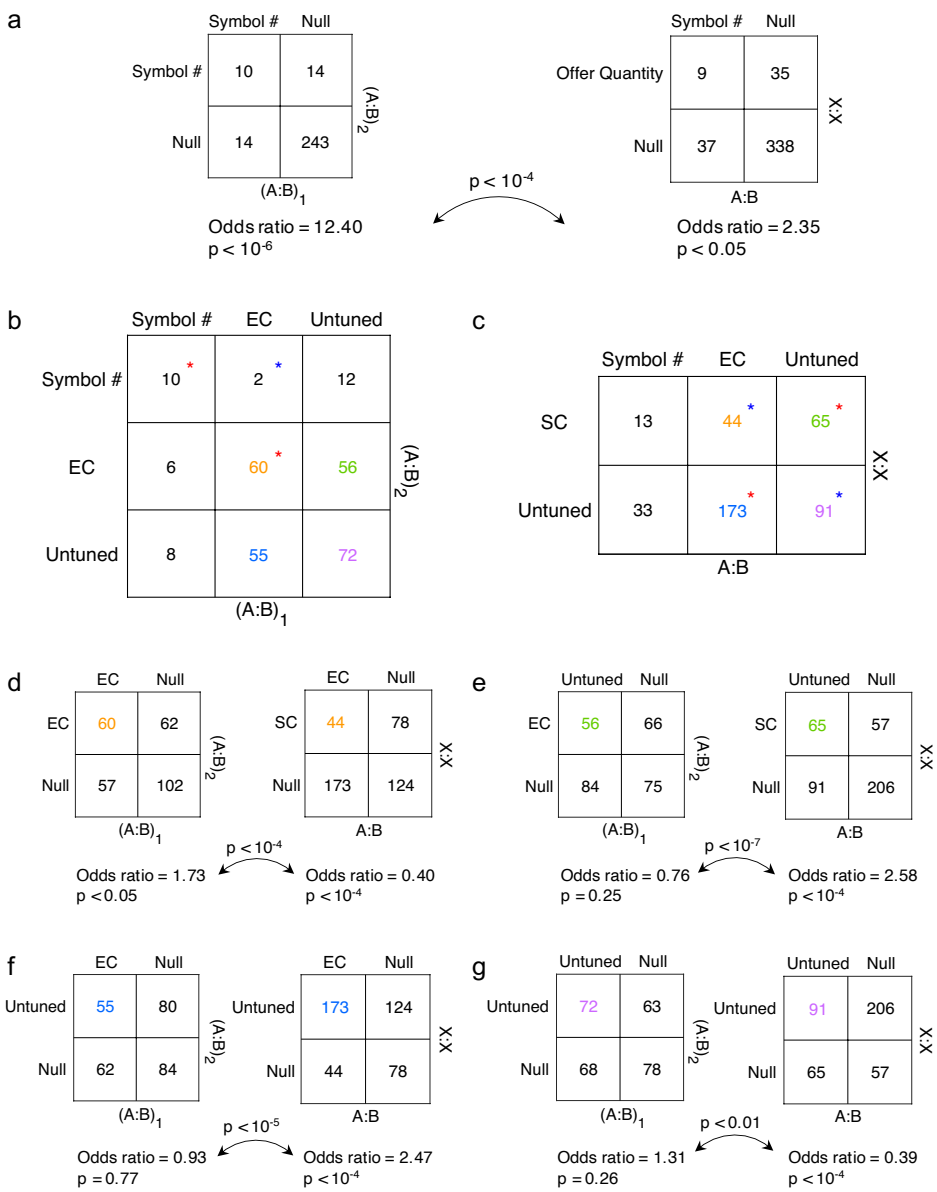

Figure 6. Contrast the remapping of encoding between $(A:B)_1 \rightarrow (A:B)_2$ and A:B→X:X conditions. (**a**) Odds ratio for {Symbol #, Offer Quantity} in A:B→X:X is significantly lower than that for {Symbol #, Symbol #} in $(A:B)_1 \rightarrow (A:B)_2$ ($p < 10^{-4}$, Z test). (**b**) Reduced contingency table, $(A:B)_1 \rightarrow (A:B)_2$ ($n = 281$). For each location, we performed Fisher's exact test. Red asterisks indicate that the cell count was significantly above chance ($p < 0.05$) while blue asterisk indicates that the cell count was significantly below chance ($p < 0.05$). EC: neurons encoding variables supporting economic choice. Task-related cells not explained by any variable were classified as untuned. (**c**) Reduced contingency table, A:B→X:X ($n = 419$). SC: neurons encoding variables supporting single attribute choice. Red asterisks indicate that the cell count was significantly above chance while blue asterisk indicates that the cell count was significantly below chance ($p < 0.05$). The odds ratios for elements of matching color in (**b**) and (**c**) were compared with a Z test in (**d**) to (**g**). (**d**) Odds ratio for {EC, SC} in A:B→X:X is significantly lower that than for {EC, EC} in $(A:B)_1 \rightarrow (A:B)_2$ ($p < 10^{-4}$, Z test). (**e**) Odds ratio for {Untuned, SC} in A:B→X:X is significantly lower than that for {Untuned, EC} in $(A:B)_1 \rightarrow (A:B)_2$ ($p < 10^{-7}$, Z test). (**f**) Odds ratio for {EC, Untuned} in A:B→X:X is significantly higher than that for {EC, Untuned} in $(A:B)_1 \rightarrow (A:B)_2$ ($p < 10^{-5}$, Z test). (**g**) Odds ratio for {Untuned, Untuned} in A:B→X:X is significantly lower than that for {Untuned, Untuned} in $(A:B)_1 \rightarrow (A:B)_2$ ($p < 0.01$, Z test).

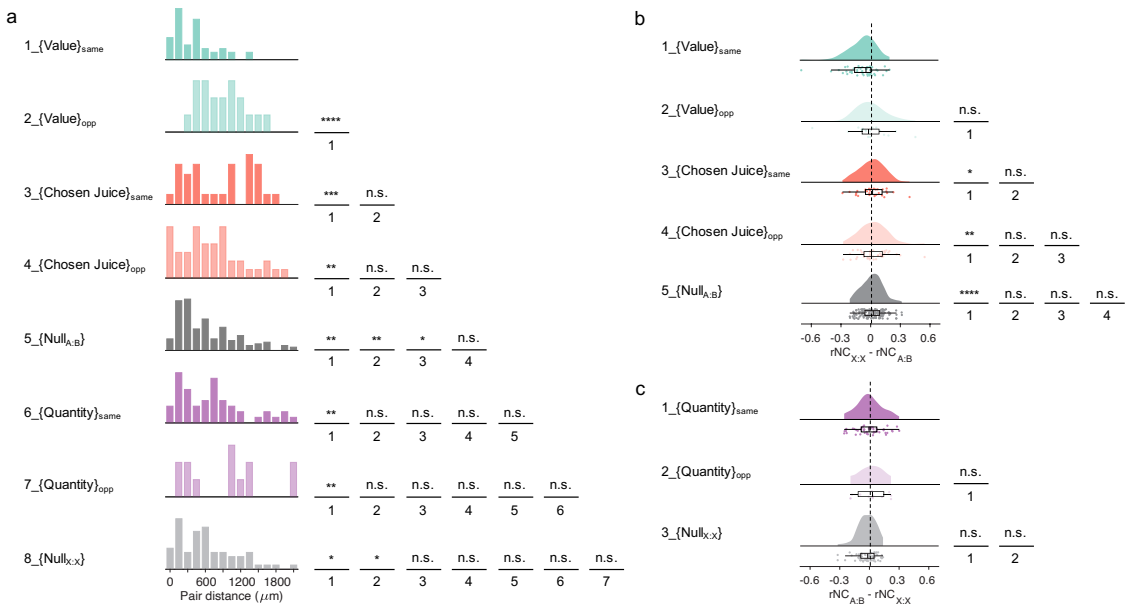

Figure 7. Pairwise distance and noise correlation analysis for task variable encoding neurons. (**a**) Distribution of cell pair distance for simultaneously recorded cell pairs encoding the *same* variable. Cells pairs with the same or opposite sign of encoding slopes were grouped separately. Cell pairs encoding Offer Value and Chosen Value in the A:B task were pooled together as $\{\text{Value}\}_{\text{same}}$ and $\{\text{Value}\}_{\text{opp}}$. Cell pairs encoding Offer Quantity and Chosen Quantity in the X:X task were pooled together as the $\{\text{Quantity}\}_{\text{same}}$ and $\{\text{Quantity}\}_{\text{opp}}$. $\{\text{Null}_{\text{A:B}}\}$ consists of randomly sampled cell pairs that were not modulated in either the A:B or X:X task. Elements in the matrix on the right indicate whether the distance between two groups is significantly different from each other. The index of each element corresponds to those indexed for each variable on the ordinate. For example, the element in the top row (****) indicates that distance of $\{\text{Value}\}_{\text{same}}$ is significantly shorter than that for $\{\text{Value}\}_{\text{opp}}$. *$p < 0.05$, **$p < 0.01$; ***$p < 0.001$, ****$p < 0.0001$; n.s., not significant (Wilcoxon Rank-Sum Test). (**b**) Change in noise correlation from A:B to X:X task ($\text{rNC}_{\text{X:X}} - \text{rNC}_{\text{A:B}}$) for cell pairs encoding the same variable in the A:B task. Dotted vertical line indicates zero on the abscissa. Elements in the matrix on the right indicate whether the change in noise correlation two groups is significantly different from each other. The index of each element corresponds to those indexed for each variable on the ordinate. *$p < 0.05$, **$p < 0.01$, ****$p < 0.0001$ (t-test). (**c**) Change in noise correlation from X:X to A:B task ($\text{rNC}_{\text{A:B}} - \text{rNC}_{\text{X:X}}$) for cell pairs encoding the same variable in the X:X task.

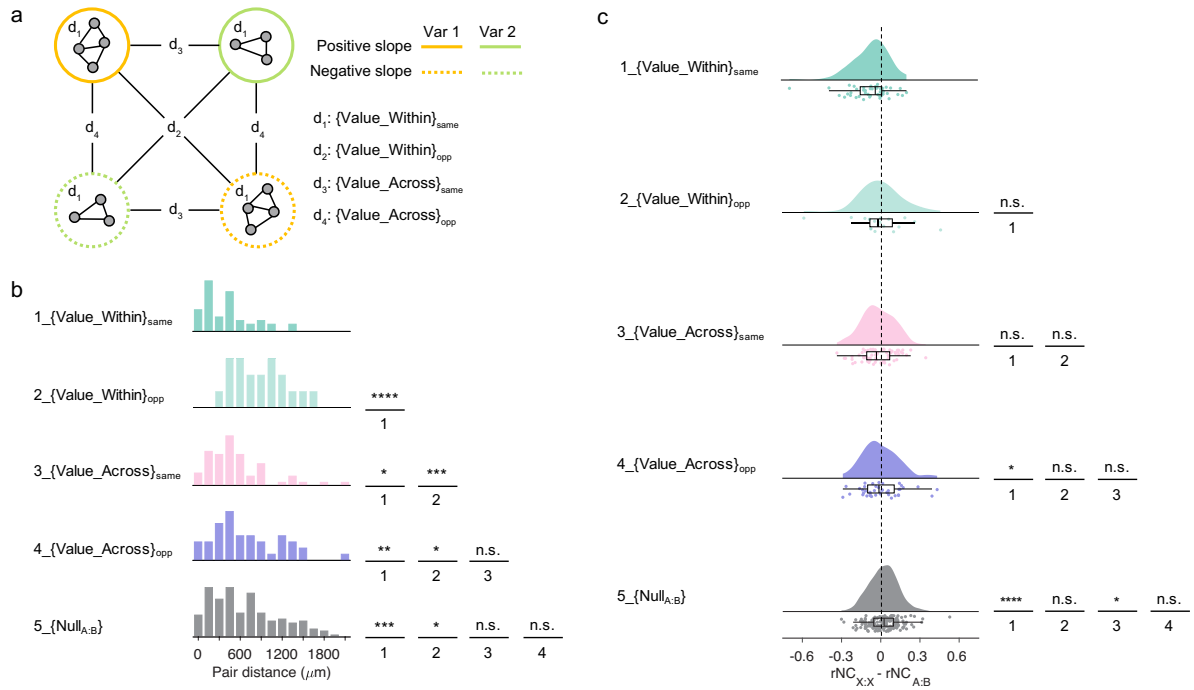

Figure 8. Pairwise distance and change in noise correlations among value coding neurons. (**a**) Pairwise distance of value coding neurons. Orange and green colors indicate neuronal populations encoding different variables while solid and dotted line patterns indicate encoding with a positive/negative regression slope. {Variable 1, Variable 2} includes the following combinations: {Offer value A, Offer value B}, {Offer value A, Chosen value} and {Offer value B, Chosen value}. d_1 stands for the pairwise distance for neurons encoding the *same* variable with the *same* sign of the encoding slope; d_2 stands for the pairwise distance for neurons encoding the *same* variable with *opposite* signs of the encoding slope; d_3 stands for the pairwise distance for neurons encoding *different* variables with the *same* sign; d_4 stands for the pairwise distance for neurons encoding *different* variables with *opposite* signs. (**b**) Distribution of pairwise distance as described in (**a**). $\{Null_{A:B}\}$ group consists of randomly sampled cell pairs that were not modulated in either the A:B or X:X task. Elements in the matrix on the right indicate whether the distance between two groups is significantly different from each other. The index of each element corresponds to those indexed for each variable on the ordinate. *$p < 0.05$; **$p < 0.01$, ***$p < 0.001$, ****$p < 0.0001$; n.s., not significant (Wilcoxon Rank-Sum Test). (**c**) Change in noise correlation ($rNC_{X:X} - rNC_{A:B}$) from A:B to X:X task for cell pairs encoding value-related variables in the A:B task. Dotted vertical line indicates zero on the abscissa. Elements in the matrix on the right indicate whether the change in noise correlation between two groups is significantly different from each other. The index of each element corresponds to those indexed for each variable on the ordinate. *$p < 0.05$, ****$p < 0.0001$; n.s., not significant (t-test).

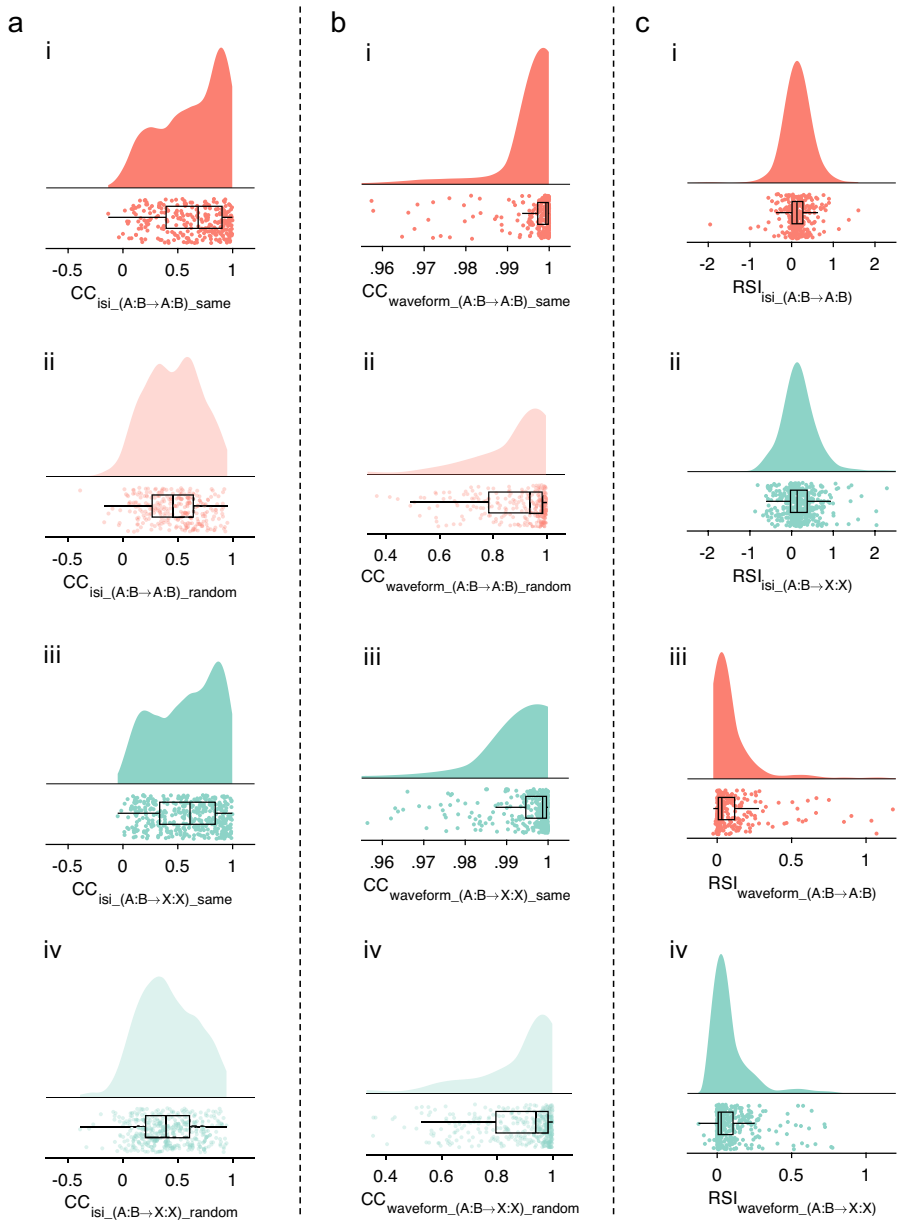

Figure S1. Metrics of recording stability. (**a**) Distribution of Pearson correlation for inter-spike intervals. (**a_i**) Distribution for the same neuron in $(A:B)_1 \rightarrow (A:B)_2$. (**a_ii**) Distribution for the same neuron in A:B→X:X. (**a_iii**) Distribution for two randomly paired different neurons in $(A:B)_1 \rightarrow (A:B)_2$. (**a_iv**) Distribution for two randomly paired different neurons in A:B→X:X. (**b**) Distribution of Pearson correlation for spike waveforms. (**b_i**) Distribution for the same neuron in $(A:B)_1 \rightarrow (A:B)_2$. (**b_ii**) Distribution for the same neuron in A:B→X:X. (**b_iii**) Distribution for two randomly paired different neurons in $(A:B)_1 \rightarrow (A:B)_2$. (**b_iv**) Distribution for two randomly paired different neurons in A:B→X:X. (**c**) Distribution of recording stability index. (**c_i**) Distribution of RSI_{isi} for $(A:B)_1 \rightarrow (A:B)_2$. (**c_ii**) Distribution of $RSI_{waveform}$ for A:B→X:X. There is no significant difference for RSI_{isi} between $(A:B)_1 \rightarrow (A:B)_2$ and A:B→X:X ($p = 0.49$, Wilcoxon Rank-Sum Test). (**c_iii**) Distribution of $RSI_{waveform}$ for $(A:B)_1 \rightarrow (A:B)_2$. (**c_iv**) Distribution of $RSI_{waveform}$ for A:B→X:X. There is no significant difference for $RSI_{waveform}$ between $(A:B)_1 \rightarrow (A:B)_2$ and A:B→X:X conditions ($p = 0.66$, Wilcoxon Rank-Sum Test).

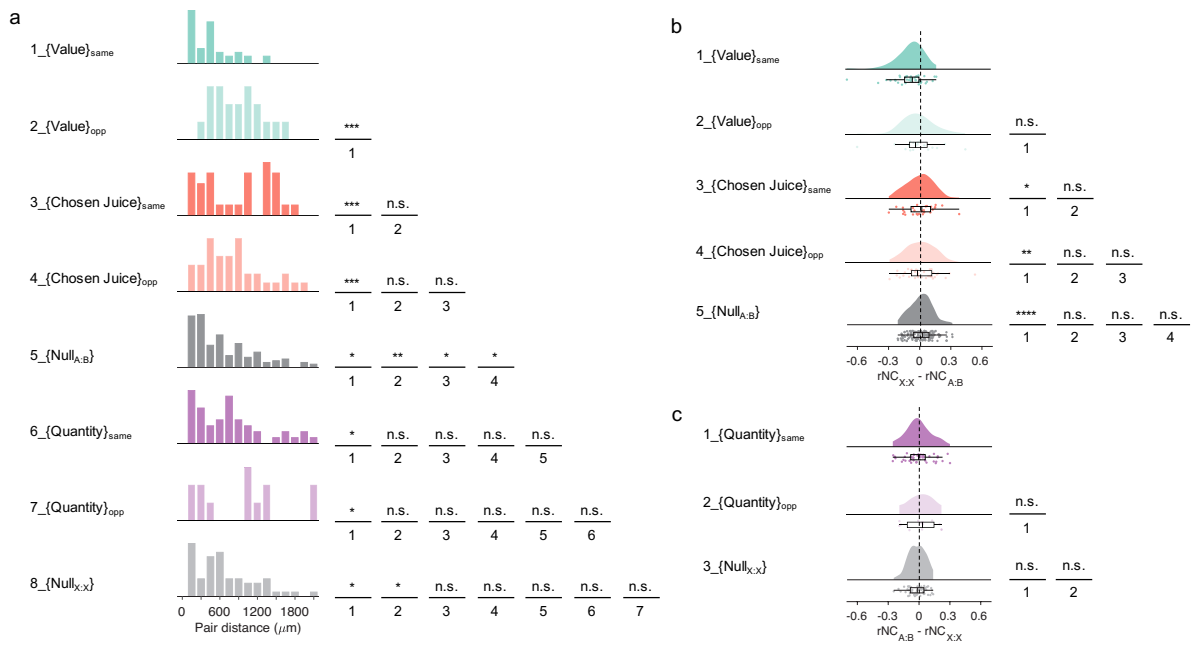

Figure S2. Same as that in **Fig. 7** but removing neuron pairs recorded from the same channel (distance = 0). *p < 0.05, **p < 0.01, ***p < 0.001; ****p < 0.0001; n.s., not significant.

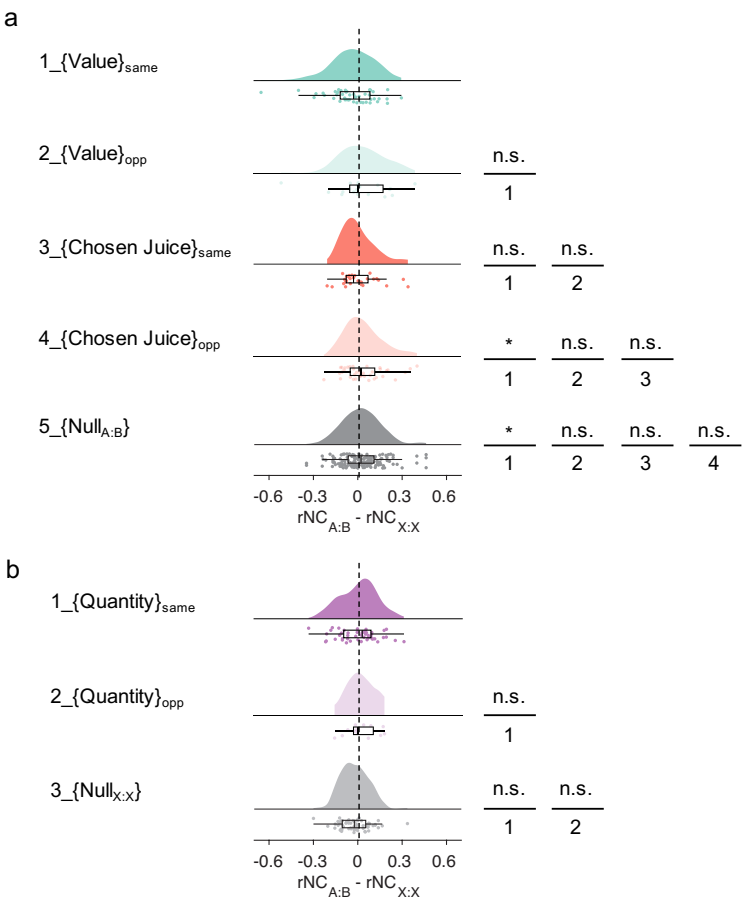

Figure S3. (**a**) Same as that in **Fig. 7b** but for post-offer window. *p < 0.05 (t-test). (**b**) Same as that in **Fig. 7c** but for the post-offer window. n.s., not significant (t-test).

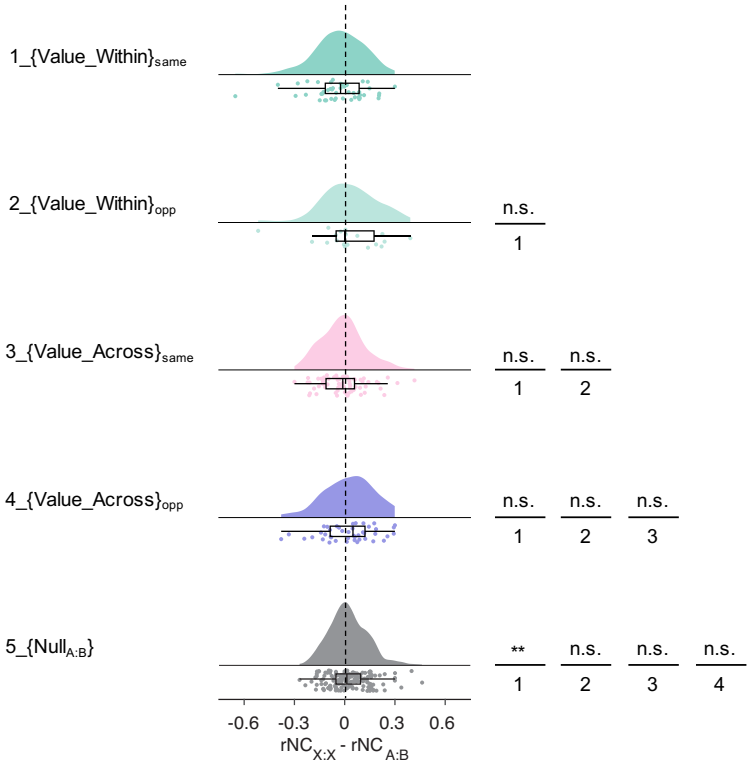

Figure S4. Same as that in **Fig. 8c** but for the post-offer window. **p < 0.01; n.s., not significant (t-test).